

# GRAPHICAL INTRODUCTION TO NLTE CHROMOSPHERIC LINE FORMATION

Invited talk at SDO-4/IRIS/Hinode Workshop, March 2012, Monterey, USA

Rob Rutten

Lingezicht Astrophysics Deil & Institutt for Teoretisk Astrofysikk Oslo

## Abstract book entry

*The basics of chromospheric line formation theory were laid out in the 1960s and 1970s by e.g., Thomas, Avrett, Hummer, Athay, Jefferies, Mihalas, Shine, Milkey. Since then there has been a long silence, without much progress in understanding the chromosphere or its diagnostics. At present, the situation changes thanks to better ground-based observing, space-based monitoring, and increasingly realistic numerical simulations. There is now a strong need to revamp classical one-dimensional static modeling as basis for chromospheric line interpretation into 3D dynamic understanding of the major diagnostics, including IRIS's Mg II h&k. In this introduction I aim to explain the old wisdom in tutorial fashion, using cartoons and graphs as means towards an intuitive grasp of facts and fallacies of chromospheric line formation.*

- [introduction](#)
- [line source function](#)
- [scattering](#)
- [partial redistribution](#)
- [1D continua](#)
- [1D lines](#)
- [canonical H \$\alpha\$](#)
- [1D H \$\alpha\$](#)
- [2D & 3D H \$\alpha\$](#)
- [conclusion and exam](#)

GRAPHICAL INTRODUCTION TO NLTE CHROMOSPHERIC LINE FORMATION  
*Invited talk at SDO-4/IRIS/Hiinode Workshop, March 2012, Monterey, USA*

Rob Rutten  
 Lingzichit Astrophysics Dept & Institut for Teoretisk Astrofysikk Oslo

Abstract book entry

The basics of chromospheric line formation theory were laid out in the 1960s and 1970s by e.g., Thomas, Avrett, Kunner, Allag, Jellicoe, Minnis, Stone, Milky. Since then there has been a long silence, without much progress in understanding the chromosphere or its diagnostics. At present, the situation changes thanks to better ground-based observing, space-based monitoring, and increasingly realistic numerical simulations. There is a new impetus to rework classical one-dimensional static modeling as basis for chromospheric line interpretation into 3D dynamic understanding of the major diagnostics, including IRIS's Mg II h & k. In this introduction I aim to explain the old wisdom in tutorial fashion, using cartoons and graphs as means towards an intuitive grasp of facts and fallacies of chromospheric line formation.

- [introduction](#)
- [line source function](#)
- [scattering](#)
- [partial redistribution](#)
- [1D continua](#)
- [1D lines](#)
- [canonical H \$\alpha\$](#)
- [1D H \$\beta\$](#)
- [3D & 3D H \$\alpha\$](#)
- [conclusion and exam](#)

The SOC asked “An intuitive approach to non-LTE diagnostics”. Meaning a mini-course on spectral lines as diagnostics of the chromosphere including IRIS’s Mg II h & k. To make this course a quickie I went graphic. Only a few equations. Hence the title.

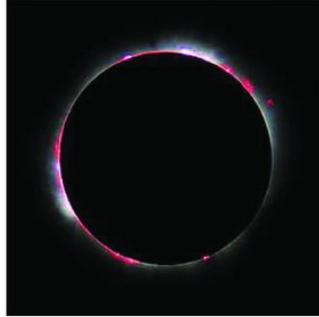
The abstract suggests that I could have given this tutorial decades ago. Correct. However, there is new insight regarding H $\alpha$  which I present towards the end. Even that bewildering line gets understood.

In this webpost of my presentation I have added tinted displays after each talk display that summarize what I said – or better, they add what I wanted to say but didn’t because of the time limit. I also replaced clickers that opened movies by weblinks for downloading, and I turned citations into weblinks that open the corresponding ADS page in your browser.

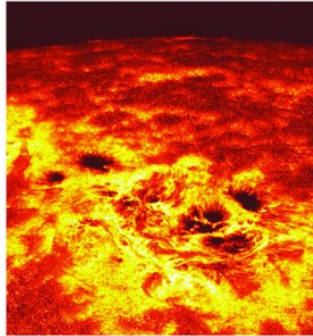
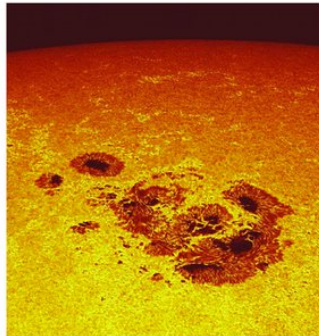
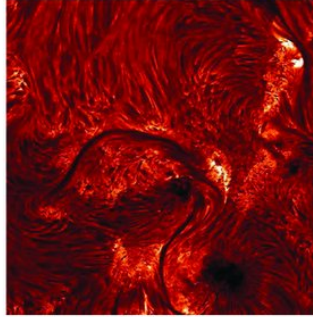
Navigation: the blue entries underneath the abstract in the previous display are clickers that jump to the corresponding parts of the talk. In each display clicking on the title or the thumbnail returns you to where you came from. Each talk display also has a hidden clicker top-left to return to the start display, and one at top-right to a thumbnail index. These are explicit in the tinted inserts, as here.

# CHROMOSPHERE

*Chromosphere at eclipse*

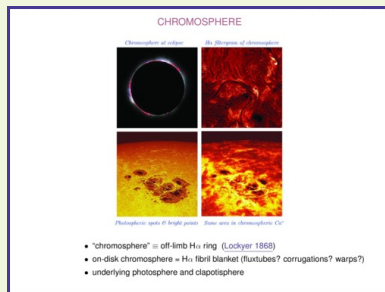


*H $\alpha$  filtergram of chromosphere*



*Photospheric spots & bright points Same area in chromospheric Ca<sup>+</sup>*

- “chromosphere”  $\equiv$  off-limb H $\alpha$  ring (Lockyer 1868)
- on-disk chromosphere = H $\alpha$  fibril blanket (fluxtubes? corrugations? warps?)
- underlying photosphere and clapotisphere



This image assembly adorned a decadal-survey White Paper by [Ayres et al. \(2009\)](#).

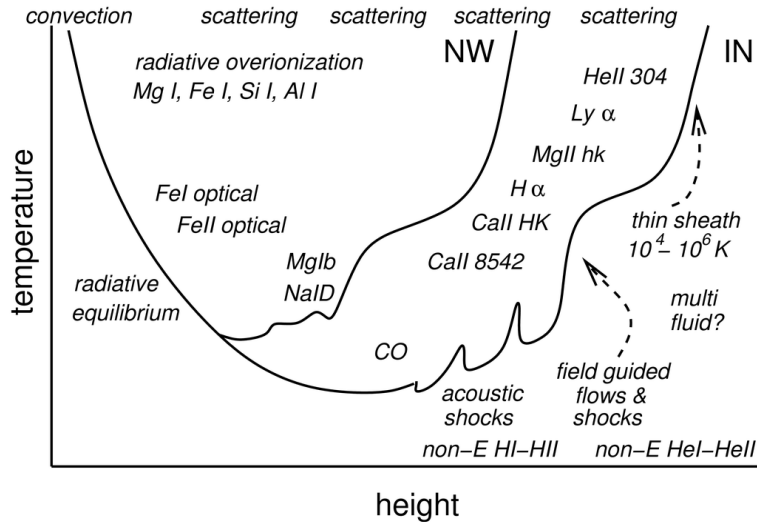
The first image illustrates the naming of the chromosphere by [Lockyer \(1868\)](#) (I typed his report into ADS). He found a pink ring around the Sun, also outside prominences, dominated by H $\alpha$ , H $\beta$ , and He I D $_3$ . The chromosphere is whatever emits these lines.

The second image, from the [DOT](#), shows the H $\alpha$  chromosphere on the disk. It is a dense mass of fibrils wherever there is a bit of activity. It is not clear whether these fibrils are cylindrical fluxtubes, ridge-shape  $\tau = 1$  corrugations, sheets, or sheet warps resembling curtain folds. They seem to outline horizontal field topography. Vertical fields are less easily seen in H $\alpha$  but are of larger interest to coronal mass and energy loading (cf. [Rutten 2012](#)). IRIS will sample these better (more below).

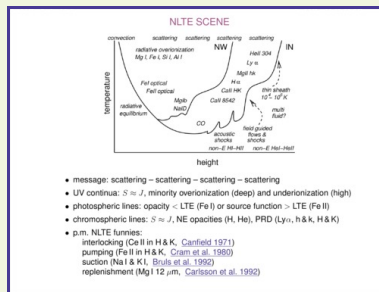
The lower-left DOT image shows the photosphere in the G band. Its bright points mark strong-field footpoints, without sign. Signed magnetograms from MDI and HMI are habitually used for field topography mapping. Since it becomes force-free only above the chromosphere, H $\alpha$  fibril patterns cannot be predicted this way. They should be monitored SDO-like and constrain NLFFF extrapolation.

The lower-right DOT image is corresponding wide-band Ca II H. It shows chromospheric emission where it is bright, elsewhere the cool shock-ridden internetwork clapotisphere underneath. I coined that kayaker name ("wild waves") just around the corner from here, in Asilomar ([Rutten 1995](#)).

# NLTE SCENE



- message: scattering – scattering – scattering – scattering
- UV continua:  $S \approx J$ , minority overionization (deep) and underionization (high)
- photospheric lines: opacity  $<$  LTE (Fe I) or source function  $>$  LTE (Fe II)
- chromospheric lines:  $S \approx J$ , NE opacities (H, He), PRD ( $\text{Ly}\alpha$ , h & k, H & K)
- p.m. NLTE funnies:
  - interlocking (Ce II in H & K, [Canfield 1971](#))
  - pumping (Fe II in H & K, [Cram et al. 1980](#))
  - suction (Na I & K I, [Bruls et al. 1992](#))
  - replenishment (Mg I 12  $\mu\text{m}$ , [Carlsson et al. 1992](#))



This cartoon shows “typical” temperature-against-height behavior for a strong-field pixel in the network (NW) and a less magnetic pixel in the internetwork (IN). The former has deep-seated shocks and a deep-seated transition to the corona. The latter has these similarly but much higher up. Each would have large temporal variation, also imposed laterally.

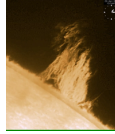
This is the scene for this tutorial. I won’t treat the listed NLTE funnies. Today the message is NLTE from scattering. For more detailed explanation see my [various course notes](#) and [lecture displays](#).

Quick overview: the photospheric temperature decline above the normal and reversed granulation (not depicted) is close to radiative equilibrium (total outward energy flux dominated by escaping radiation).

The ultraviolet electron-donor continua of Mg I, Fe I, Si I, and Al I (minority species which set the free electron density for the  $H^-$  continuous opacity at  $N_e \approx 10^{-4} N_H$ ) are much out of LTE due to bound-free scattering, with  $S_\nu \approx J_\nu > B_\nu$  in the photosphere and  $S_\nu \approx J_\nu < B_\nu$  higher up. As a result, their photospheric lines tend to have smaller-than-LTE opacities but LTE source functions. Photospheric lines from majority species such as Fe II tend to have LTE opacities but superthermal source functions.

The stronger lines formed in the chromosphere (note that Mg I b and Na I D are largely photospheric) are all strong scatterers with  $S_\nu \approx J_\nu$ . My main topic here. Additional complexity is given by partial frequency redistribution (PRD) and non-equilibrium (NE) hydrogen and helium ionization.

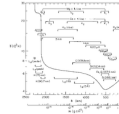
# WHO WANTS TO KNOW WHAT WHAT FOR?



- *optically thin cloud modeler*

courtesy Tom Berger

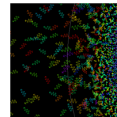
- $I_\nu(\tau_\nu) = I_\nu(0) e^{-\tau_\nu} + \int_0^{\tau_\nu} S_\nu(t_\nu) e^{-(\tau_\nu - t_\nu)} dt_\nu \approx I_\nu(0) e^{-\tau_\nu(D)} + S_\nu (1 - e^{-\tau_\nu(D)})$
- off limb:  $I_\nu(0) = 0$  but how do I solve confusion?
- on disk: how do I define the unseen  $I_\nu(0)$ ?



- *optically thick Eddington-Barbier inverter*

courtesy Gene Avrett

- $I_\nu^+(\tau_\nu=0, \mu) = \int_0^\infty S_\nu(t_\nu) e^{-t_\nu/\mu} dt_\nu/\mu \approx S_\nu(\tau_\nu=\mu)$
- can I get away with  $\tau_\nu = \tau_\nu^{\text{LTE}}$  and  $S_\nu = B_\nu$ ?
- at what height does my line form and how does it tell me  $T, N_e, \vec{v}, \vec{B}$ ?



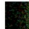


- *excitable atom in the solar atmosphere*

courtesy Mats Carlsson

- what colliders and photons are available for my excitation?
- shall I emit or extinct a photon in the observer's direction?
- do I muck with coherency?

WHO WANTS TO KNOW WHAT WHAT FOR?

- 
 • optically thin cloud modeler courtesy Tom Berger
  - $I_{\nu}(r_{\nu}) = I_{\nu}(0) e^{-\tau_{\nu}} + \int_0^{\tau_{\nu}} S_{\nu}(t_{\nu}) e^{-(\tau_{\nu}-t_{\nu})} dt_{\nu} \approx I_{\nu}(0) e^{-\tau_{\nu}(1+\beta)} + S_{\nu}(1 - e^{-\tau_{\nu}(1+\beta)})$
  - off limb:  $I_{\nu}(0) = 0$  but how do I solve confusion?
  - on disk: how do I define the unseen  $I_{\nu}(0)$ ?
- 
 • optically thick Eddington-Barbier inverter courtesy Gene Avrett
  - $I'_{\nu}(\tau_{\nu} = 0, \mu) = \int_0^{\tau_{\nu}} S_{\nu}(t_{\nu}) e^{-t_{\nu}/\mu} dt_{\nu} \mu \approx S_{\nu}(\tau_{\nu} = \mu)$
  - can I get away with  $\tau_{\nu} = \tau_{\nu}^{\text{LTE}}$  and  $S_{\nu} = B_{\nu}$ ?
  - at what height does my line form and how does it tell me  $T_e, N_e, \rho, \beta$ ?
- 
 • excitable atom in the solar atmosphere courtesy Mats Carlsson
  - what colliders and photons are available for my excitation?
  - shall I emit or extinct a photon in the observer's direction?
  - do I muck with coherency?

The first clicker opened [this beautiful Tom Berger prominence movie](#). Cloud modeling was established in [Beckers's](#) (1964) [PhD thesis](#) (which I have put on ADS). In Hinode's  $H\alpha$  the filament threads appear optically thin, but they are likely very thick in  $Ly\alpha$  with scattered  $Ly\alpha$  radiation governing  $H\alpha$  opacities. Single-line cloud modeling therefore gets replaced with multi-line multi-thread modeling (e.g., [Gunár et al. 2011](#)).

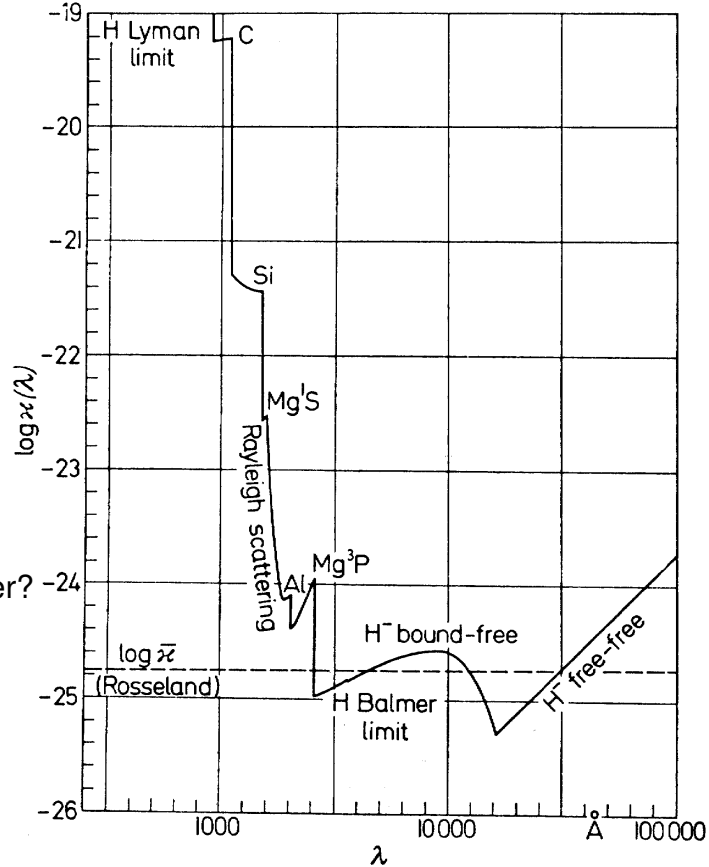
The second clicker opened Gene Avrett's famous [VALIIC](#) temperature-height plot with height-of-formation ranges for many spectral diagnostics. (He reversed the height scale; in this talk height increases to the right and so does optical depth, be aware that the outward direction flips between the two.) Eddington-Barbier estimation for height of formation is often instructive for optically thick media but can be [dangerous](#). Photospheric Fe I 6303 Å Stokes inversion codes typically assume  $S_{\nu} = B_{\nu}$  reasonably correctly but  $\tau_{\nu} = \tau_{\nu}^{\text{LTE}}$  wrongly ([Rutten 1988](#), [Shchukina & Trujillo Bueno 2001](#)).

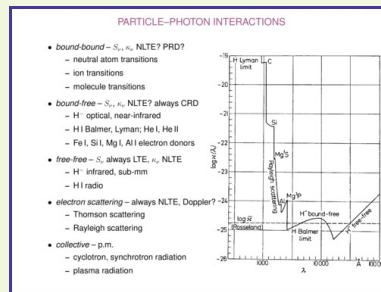
The third clicker opened [Mats Carlsson's](#) illustration for the poster announcing the 1995 Oslo summer school which also adorns my [graduate-level lecture notes](#). It shows photons getting scarcer, longer, redder, more outwards directed on the way out. That is the radiative transfer part. We must also question how atoms feel about photons. In simple thin conditions, such as coronal EUV line formation, the atom feeling suffices. For the chromosphere photon scattering adds transfer complexity that many thin-type astronomers shy away from. My mission here is to make you like it.



# PARTICLE-PHOTON INTERACTIONS

- *bound-bound* –  $S_\nu, \kappa_\nu$  NLTE? PRD?
  - neutral atom transitions
  - ion transitions
  - molecule transitions
- *bound-free* –  $S_\nu, \kappa_\nu$  NLTE? always GRD
  - $H^-$  optical, near-infrared
  - H I Balmer, Lyman; He I, He II
  - Fe I, Si I, Mg I, Al I electron donors
- *free-free* –  $S_\nu$  always LTE,  $\kappa_\nu$  NLTE
  - $H^-$  infrared, sub-mm
  - H I radio
- *electron scattering* – always NLTE, Doppler?
  - Thomson scattering
  - Rayleigh scattering
- *collective* – p.m.
  - cyclotron, synchrotron radiation
  - plasma radiation





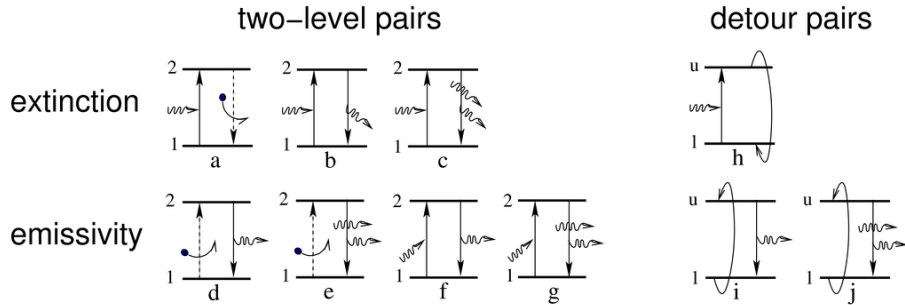
Overview of how particles and photons feel each other. The graph of continuous opacity against wavelength at photospheric height is a didactic rendering by E. Böhm-Vitense of her classic confusograms in [Vitense \(1951\)](#).

The visual and infrared are dominated by  $H_{\text{bf}}^-$  and  $H_{\text{ff}}^-$  thanks to the photosphere being one of the unusual locations in the universe where hydrogen is neutral. The extra electrons come from abundant metals with low ionization energy (“electron donors”). Because the sun is a metal-rich star and these metals are nearly fully ionized, they provide  $N_e \approx 10^{-4} N_H$  where hydrogen is neutral. And so provide the solar continuum opacity that was as large a riddle to [Eddington \(1926\)](#) as solar energy generation (“two clouds obscuring the theory of the stars”).

The electron-donor ionization edges dominate in the ultraviolet and are formed much out of LTE, both in source function and in opacity ([shown below for Mg I](#)). They form in the photosphere.

Bound-bound transitions can provide enormous extra line opacity (“extinction”: both absorption and scattering count) on top of the continuous opacity. The strongest ones provide lines formed in the chromosphere, meaning that chromospheric fibrils are opaque in them (lingo: a line cannot be optically thick, something can be thick in a line). The strongest of all is  $Ly\alpha$ , not detailed here since IRIS will not observe it. This tutorial concerns the NLTE and PRD aspects of optical chromosphere lines and Mg II h & k, with special attention for new results on  $H\alpha$ . The message is scattering.

# LINE FORMATION AS SEEN BY THE ATOM



- *pair combinations*

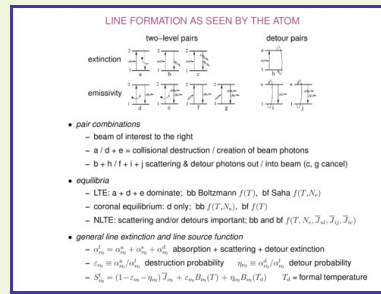
- beam of interest to the right
- a / d + e = collisional destruction / creation of beam photons
- b + h / f + i + j scattering & detour photons out / into beam (c, g cancel)

- *equilibria*

- LTE: a + d + e dominate; bb Boltzmann  $f(T)$ , bf Saha  $f(T, N_e)$
- coronal equilibrium: d only; bb  $f(T, N_e)$ , bf  $f(T)$
- NLTE: scattering and/or detours important; bb and bf  $f(T, N_e, \bar{J}_{ul}, \bar{J}_{ij}, \bar{J}_{ic})$

- *general line extinction and line source function*

- $\alpha_{\nu_0}^l = \alpha_{\nu_0}^a + \alpha_{\nu_0}^s + \alpha_{\nu_0}^d$  absorption + scattering + detour extinction
- $\varepsilon_{\nu_0} \equiv \alpha_{\nu_0}^a / \alpha_{\nu_0}^l$  destruction probability       $\eta_{\nu_0} \equiv \alpha_{\nu_0}^d / \alpha_{\nu_0}^l$  detour probability
- $S_{\nu_0}^l = (1 - \varepsilon_{\nu_0} - \eta_{\nu_0}) \bar{J}_{\nu_0} + \varepsilon_{\nu_0} B_{\nu_0}(T) + \eta_{\nu_0} B_{\nu_0}(T_d)$        $T_d =$  formal temperature



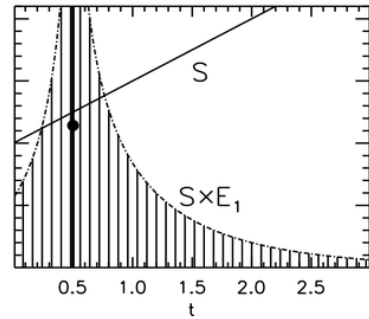
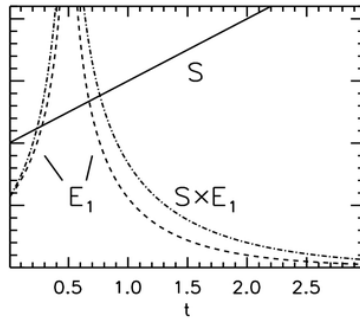
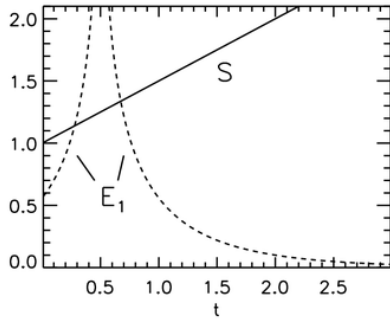
The atom point of view. The cartoons combine the atomic processes involving line photons in pairs, those contributing line extinction in the upper row, line emissivity in the lower row. The beam direction is to the right. Similar cartoons hold for bound-free transitions. The seven pairs at left describe two-level atoms in which any excitation is necessarily followed by deexcitation in the same bound-bound transition. Induced scattering pairs c (out of the beam) and g (into the beam) cancel (see [essay by Rutten 2003](#)). The three pairs at right describe “interlocking” multi-level detour paths, with the curved arrows representing summations over all indirect collisional and/or radiative pathways from upper to lower level or vice-versa. These may include bound-free excursions.

In the deep photosphere the collision density is large enough that beam photon destruction (a) and creation (d + e) dominate. In the tenuous chromosphere scattering (b out of, e + f into the beam) and detours (h out of, i + j into the beam) dominate instead. Coronal equilibrium is just like pair d with the created photon either observed (into the beam) or lost (out of the beam). Opposite to LTE (Boltzmann, Saha), coronal-equilibrium lines have  $(T, N_e)$  dependence, ionization continua  $T$ -only dependence.

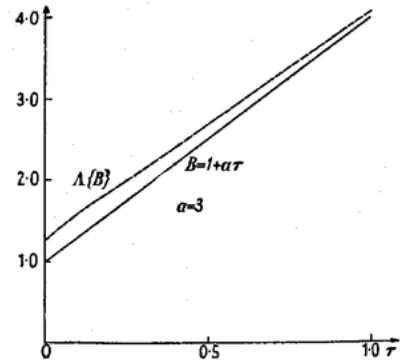
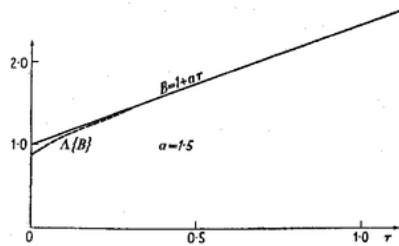
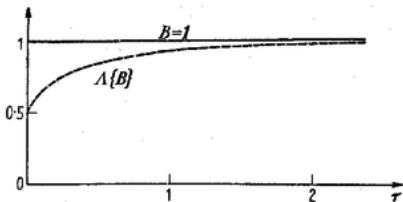
The general CRD line source function combining all pairs is given at the bottom.  $\bar{J}_{\nu_0} \equiv (1/4\pi) \int_0^{\infty} \int_0^{4\pi} \varphi(\nu - \nu_0) I_{\nu} d\Omega d\nu$  is the profile-averaged angle-averaged radiation from elsewhere, a non-local term.  $T_d$  is a formal temperature describing the combined detour rates. The terms with detour probability  $\eta_{\nu_0}$  vanish for a two-level-atom gas yielding  $S_{\nu_0}^l = (1 - \epsilon_{\nu_0}) \bar{J}_{\nu_0} + \epsilon_{\nu_0} B_{\nu_0}(T)$ .

# RADIATION FROM ELSEWHERE: THE $\Lambda$ OPERATOR

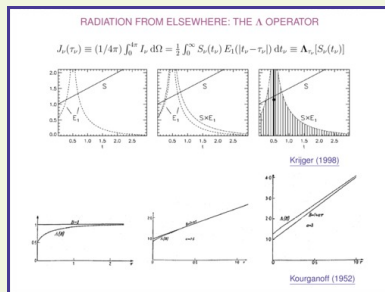
$$J_\nu(\tau_\nu) \equiv (1/4\pi) \int_0^{4\pi} I_\nu d\Omega = \frac{1}{2} \int_0^\infty S_\nu(t_\nu) E_1(|t_\nu - \tau_\nu|) dt_\nu \equiv \Lambda_{\tau_\nu}[S_\nu(t_\nu)]$$



Krijger (1998)



Kourganoff (1952)



The Schwarzschild equation for a plane-parallel atmosphere with  $E_1(x) \equiv \int_0^1 e^{-x/\mu} (1/\mu) d\mu$  defines the  $\Lambda$  operator. [Thijs Krijger's](#) graphs illustrate its working. Specify  $S(t)$ . Overplot  $E_1(|t - \tau|)$  at the depth of interest ( $\tau = 0.5$ ). Do the multiplication. The tilt of  $S(t)$  produces asymmetry between the two tails. Do the integral (area summation) and divide by 2 to get the mean of the two tail areas. The bullet specifies the resulting  $J(0.5)$ . It lies below  $S(0.5)$  because the lefthand tail is cut off at the surface whereas the righthand tail continues beyond the plot boundary to  $t = \infty$ . For deeper sampling the result gets closer to  $S$  because the outer cut-off part diminishes. Linear  $S(t)$  there produces linear intensity anisotropy (apply Eddington-Barbier for  $\Delta t = \pm\mu$  around  $t = \tau$ ) that cancels in the  $J$  averaging.

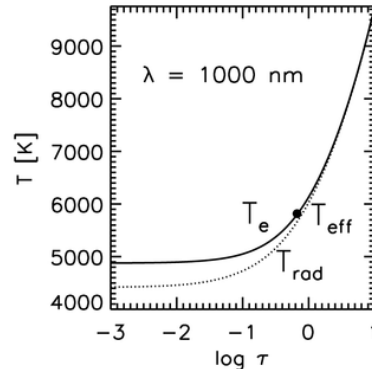
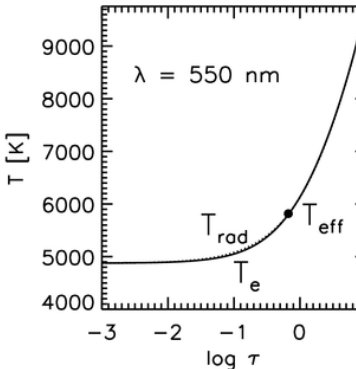
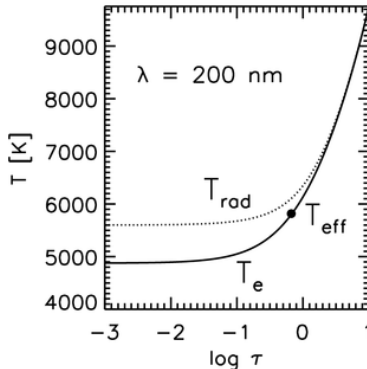
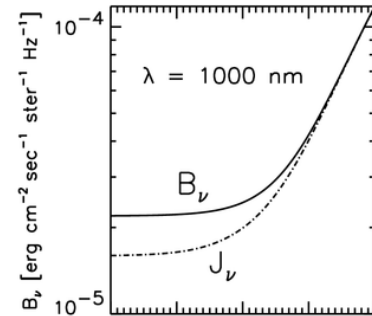
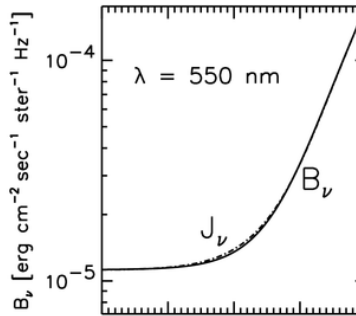
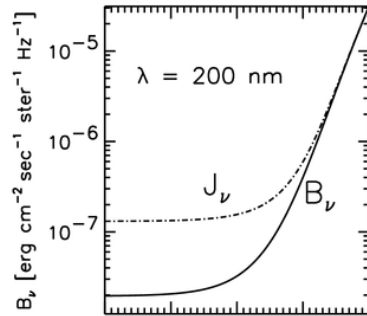
If  $S(t)$  is constant then  $J(0) = 0.5 S$ . Obvious: the Eddington-Barbier approximation, exact for linear  $S(t)$ , then says that  $I^+(0, \mu) = S(\tau = \mu) = S$  in any outward direction (Lambert radiator). There is no inward  $I^-$  at the surface, so the angle averaging over all directions gives  $0.5 I^+$ . This case is shown in the first Kourganoff graph (with the source function written as  $B$  for LTE).

When  $S(t)$  increases steeply inward the righthand tail wins from the cut-off lefthand tail making  $J > S$  near the surface. This is shown in the third Kourganoff graph. The second graph illustrates the radiative-equilibrium gradient  $S = 1 + (3/2) t$  producing  $J \approx S$ .

Upshot: steep  $S(\tau)$  produces  $J > S$  near the surface, shallow  $S(\tau)$  produces  $J < S$  near the surface. With wide contribution kernels. At larger depth  $J \rightarrow S$ .

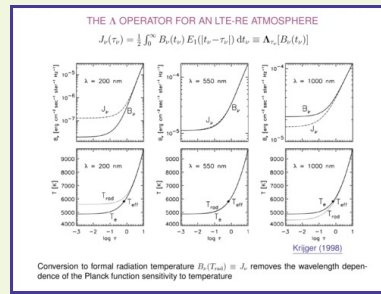
# THE $\Lambda$ OPERATOR FOR AN LTE-RE ATMOSPHERE

$$J_\nu(\tau_\nu) = \frac{1}{2} \int_0^\infty B_\nu(t_\nu) E_1(|t_\nu - \tau_\nu|) dt_\nu \equiv \Lambda_{\tau_\nu}[B_\nu(t_\nu)]$$



[Krijger \(1998\)](#)

Conversion to formal radiation temperature  $B_\nu(T_{rad}) \equiv J_\nu$  removes the wavelength dependence of the Planck function sensitivity to temperature



The Schwarzschild equation for LTE with  $S_\nu(\tau) = B_\nu[T(\tau)]$ .

Krijger's plots are for a grey LTE Milne-Eddington atmosphere with solar effective temperature and radiative-equilibrium stratification  $T(\tau) = T_{\text{eff}} [(1 + (3/2)\tau)/2]^{1/4}$ . The upper plots show  $B_\nu$  and  $J_\nu$  against depth, the lower plots the corresponding formal temperatures. The latter are better suited for different-wavelength comparison by sharing the same y-axis extent.

Since the bulk of the flux comes out in the visual the center panels have  $J_\nu \approx B_\nu$  to produce the spectrum-wide  $\int_0^\infty \kappa_\nu (S_\nu - J_\nu) d\nu = 0$  radiative equilibrium condition.

At short wavelengths the larger Wien response of the Planck function to temperature causes steeper  $B_\nu(\tau)$  increase and therefore  $J_\nu > B_\nu$ . Note the large y-axis range of the upper-left panel.

At long wavelengths the Planck function has only linear Rayleigh-Jeans sensitivity to the temperature so that the  $B_\nu(\tau)$  gradient is much less steep, resulting in  $J_\nu < B_\nu$ .

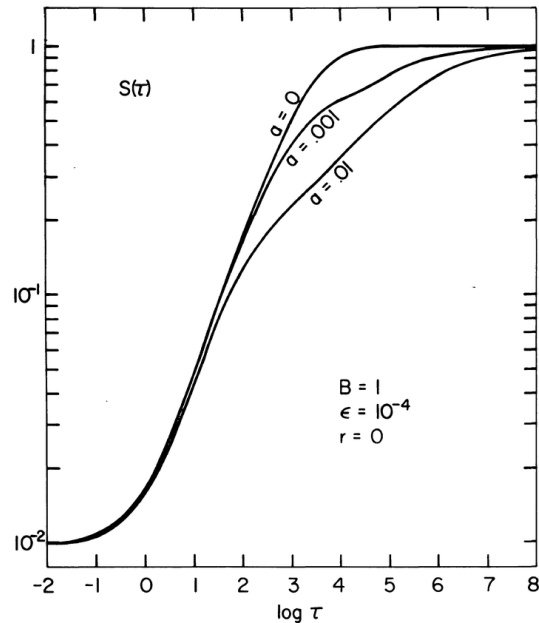
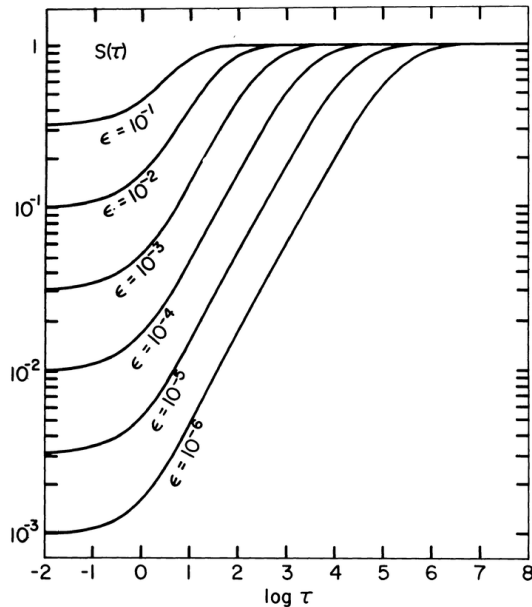
Upshot: upper-photosphere continua have  $J_\nu > B_\nu$  at short wavelengths,  $J_\nu < B_\nu$  at long wavelengths, already in the absence of scattering.



# SCATTERING IN AN ISOTHERMAL CONSTANT-EPSILON ATMOSPHERE

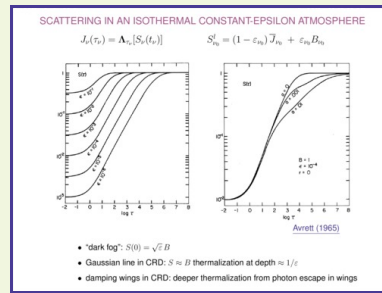
$$J_\nu(\tau_\nu) = \Lambda_{\tau_\nu}[S_\nu(t_\nu)]$$

$$S_{\nu_0}^l = (1 - \varepsilon_{\nu_0}) \bar{J}_{\nu_0} + \varepsilon_{\nu_0} B_{\nu_0}$$



[Avrett \(1965\)](#)

- “dark fog”:  $S(0) = \sqrt{\varepsilon} B$
- Gaussian line in CRD:  $S \approx B$  thermalization at depth  $\approx 1/\varepsilon$
- damping wings in CRD: deeper thermalization from photon escape in wings



The Schwarzschild and two-level-scattering equations together govern the behavior of  $S$  and  $J$ . Avrett's classic graphs are for an isothermal homogeneous two-level-atom gas with constant collisional photon destruction probability per extinction  $\epsilon$ , assuming complete frequency redistribution (CRD; no coherency = no monochromaticity in scattering up-down pairs; more below).

For LTE  $\epsilon = 1$ ,  $S(0) = B \equiv 1$ ,  $J(0) = 0.5 S$ . The surface is a half-isotropic Lambert radiator.

For smaller  $\epsilon$  the surface value  $S(0)$  goes down following the  $\sqrt{\epsilon}$  law. The emergent intensity  $I(0) \approx S(\tau = 1)$  becomes very low, about  $3\sqrt{\epsilon} B$ . As in fog diluting the intensity of a street light. If you add a thin layer to the atmosphere it will scatter photons back without creating as many new ones.

In deep layers the radiation field isn't aware yet that photons can escape. There the radiation field is only linearly anisotropic with  $\bar{J} \approx B$ . In a real atmosphere with density stratification  $\epsilon \rightarrow 1$  with depth since the collision frequency increases. Both make  $S \rightarrow B$  with depth.

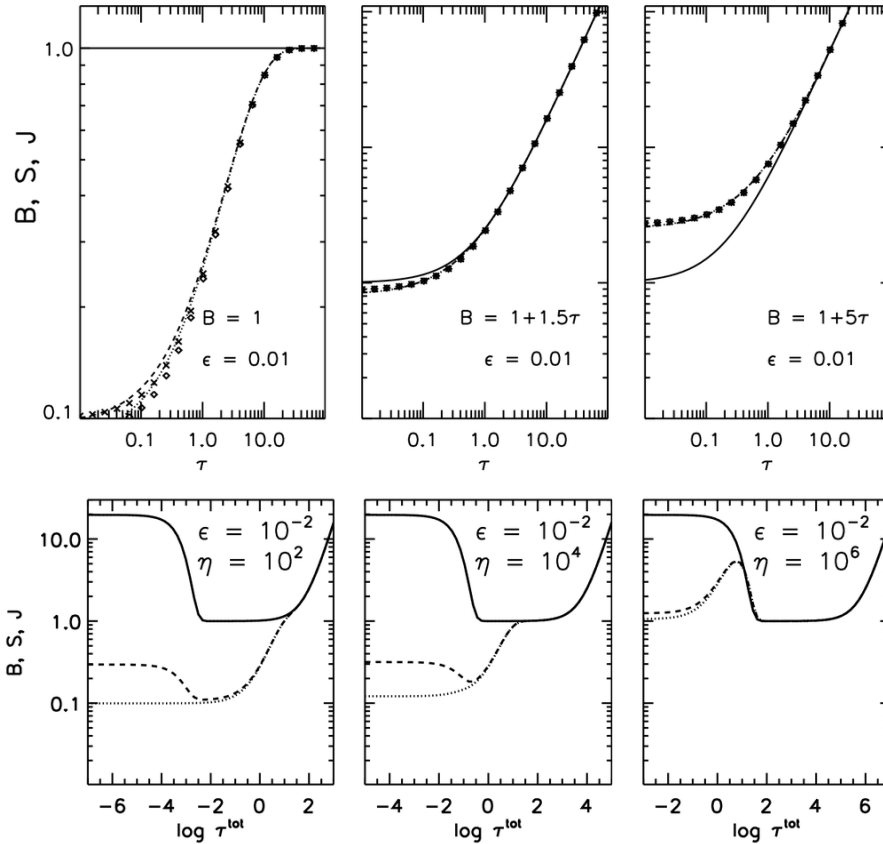
At more scattering the knowledge that there is an escape surface propagates inward. The "thermalization depth" where  $S \approx B$  is at  $\tau = 1/\epsilon$  for CRD and constant  $\epsilon$ . If the line has damping wings the thermalization deepens further (righthand plot) because photons have larger escape probability in the extended low-opacity wings.

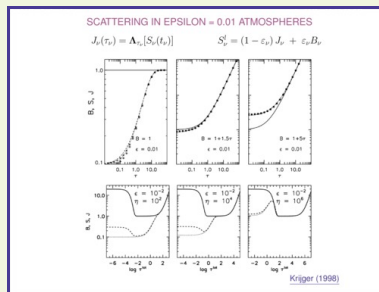
Upshot: scattering darkens the emergent intensity and deepens the thermalization tremendously.

# SCATTERING IN EPSILON = 0.01 ATMOSPHERES

$$J_\nu(\tau_\nu) = \Lambda_{\tau_\nu}[S_\nu(t_\nu)]$$

$$S_\nu^l = (1 - \epsilon_\nu) J_\nu + \epsilon_\nu B_\nu$$





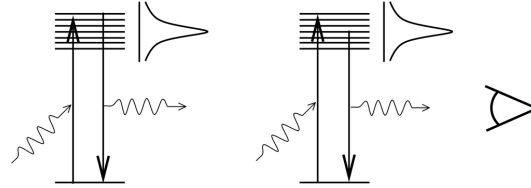
Again the Schwarzschild and two-level-scattering equations, now for coherent scattering (no bar on  $J$ ). Again two-level-atom gas, with depth-independent destruction probability  $\epsilon = 10^{-2}$ .  $B, S, J$  curves against depth (solid, dashed, dotted). Diamonds and crosses:  $J$  and  $S$  from the Eddington approximation which assumes linearly anisotropic intensity. It is pretty good.

Upper row: linear  $B(\tau)$  gradients. The first panel for the isothermal case is similar to the  $\epsilon = 10^{-2}$  of [Avrett's graph](#), except that thermalization occurs at  $\tau \approx 1/\sqrt{\epsilon}$  because here coherent (monochromatic) scattering is assumed. The second panel has the radiative-equilibrium gradient producing  $S \approx J \approx B$ . The third panel has a steep Planck-function gradient, also with thermalisation at  $\tau \approx 1/\sqrt{\epsilon}$  but less evident because all three curves drop steeply.

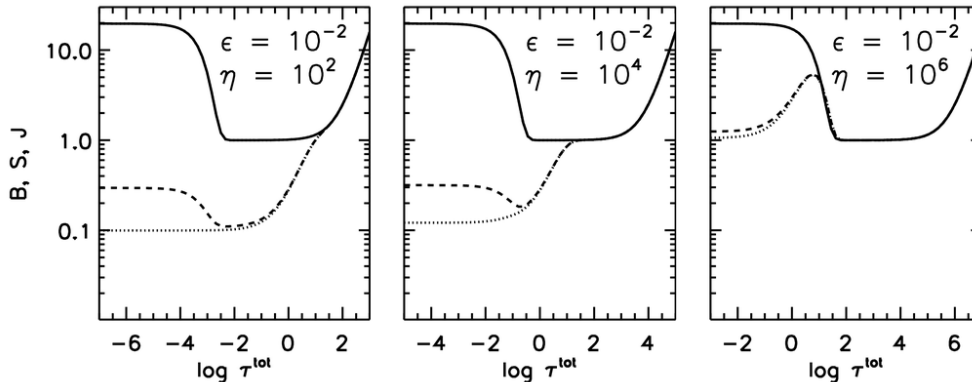
Lower row: sort-of-solar temperature stratification with a radiative-equilibrium photosphere, a flat temperature minimum, and a chromospheric temperature rise. Parameter  $\eta$  is the line-to-continuum extinction ratio  $\kappa^l/\kappa^c$ , also assumed depth-independent. For stronger lines  $J$  and  $S$  decouple further out from  $B$ . In each case they drop away from that point. For this rather large  $\epsilon$  the source function still senses the chromospheric temperature rise.

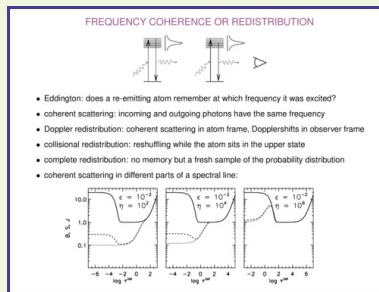
Strong lines do not have  $J > B$  even at short wavelengths where continua do, because their gradient  $dS/d\tau = dS/(\kappa^l + \kappa^c) dz = dS/(1 + \eta) d\tau^c$  is much less steep than  $dS/d\tau^c$ . Strong lines therefore tend to the isothermal case.

# FREQUENCY COHERENCE OR REDISTRIBUTION



- Eddington: does a re-emitting atom remember at which frequency it was excited?
- coherent scattering: incoming and outgoing photons have the same frequency
- Doppler redistribution: coherent scattering in atom frame, Dopplershifts in observer frame
- collisional redistribution: reshuffling while the atom sits in the upper state
- complete redistribution: no memory but a fresh sample of the probability distribution
- coherent scattering in different parts of a spectral line:





*Cartoons: resonance scattering into the beam for a transition with a sharp (infinite lifetime) lower level. The upper level may be regarded as widened according to the extinction profile. In coherent (monofrequent, monochromatic) scattering the outgoing photon has precisely the same frequency as the incoming one. In complete redistribution (CRD) the outgoing photon samples the profile function.*

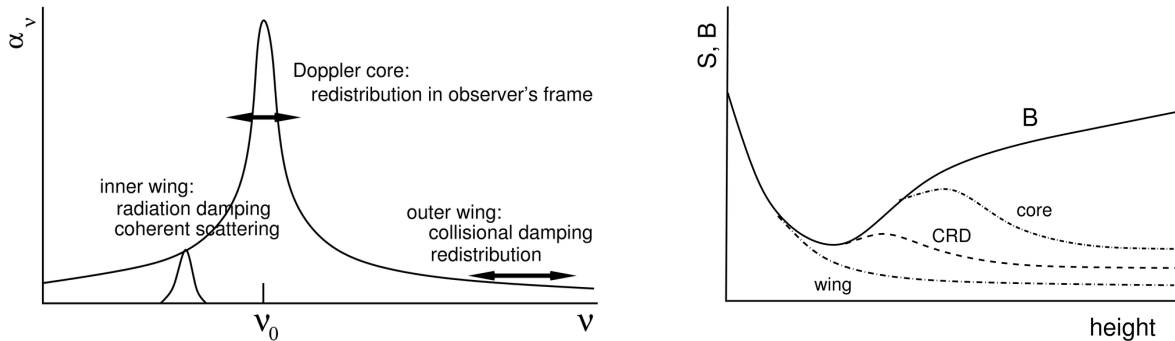
*Doppler redistribution occurs over the Doppler width in the frame of the observer for coherent scattering in the frame of the atom. Systematic motion may upset this Maxwellian ensemble notion, making addition of “microturbulence” even more suspect than it is already.*

*Collisional redistribution may be described as wavetrain phase jumps from abrupt encounters in the impact approximation, or as term-diagram morphing by nearest-neighbor charges in the quasi-static approximation. Obviously more important at larger collider/neighbor density, hence deeper in the atmosphere.*

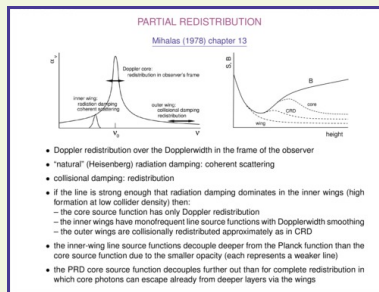
*Graphs: the same as on the [previous talk display](#). Now they may be interpreted as illustrating the effects of coherent scattering in the core, inner, and outer wing of a strong line. Each part of the line has its own monochromatic thermalization depth and its own corresponding frequency-dependent source function behavior.*

# PARTIAL REDISTRIBUTION

Mihalas (1978) chapter 13



- Doppler redistribution over the Dopplerwidth in the frame of the observer
- “natural” (Heisenberg) radiation damping: coherent scattering
- collisional damping: redistribution
- if the line is strong enough that radiation damping dominates in the inner wings (high formation at low collider density) then:
  - the core source function has only Doppler redistribution
  - the inner wings have monofrequent line source functions with Dopplerwidth smoothing
  - the outer wings are collisionally redistributed approximately as in CRD
- the inner-wing line source functions decouple deeper from the Planck function than the core source function due to the smaller opacity (each represents a weaker line)
- the PRD core source function decouples further out than for complete redistribution in which core photons can escape already from deeper layers via the wings



*Lefthand cartoon: partial coherency across the extinction profile. Doppler redistribution occurs in the frame of the observer for coherent scattering in the frame of the atom. It causes redistribution over the Doppler core. The outer wings are usually formed so deep in the atmosphere that the large collision frequency (or nearest-neighbor density) there causes collisional redistribution. The inner wings, when dominated by natural damping (Heisenberg uncertainty principle), scatter coherently, again with Doppler redistribution for the observer.*

*Righthand cartoon: in PRD the Doppler core, inner wing parts, and the outer wings represent independent photon ensembles. Each scatters outward in its own manner, each with its source function decoupling from the Planck function at its own thermalization height. With deeper decoupling and escape further into the wings.*

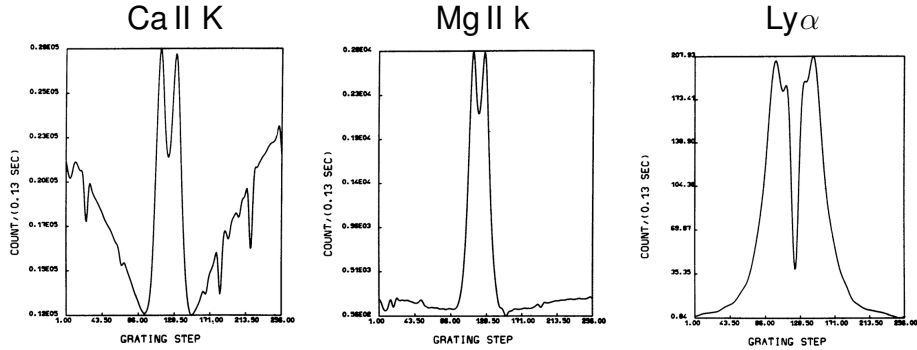
*The CRD source function represents a sort of frequency average over the whole profile and so decouples higher than the PRD wings, lower than the PRD core.*

*Personal note: my nestor [Jaap Houtgast](#) wrote a famous [thesis](#) in 1942 about complete redistribution in Fraunhofer lines. He took me to three solar eclipses; the third provided [my thesis](#) material on coherency in Ba II 4554 Å. My first graduate student, [Han Uitenbroek](#), addressed cross-redistribution between Ca II H & K and the Ca II IR lines in [his thesis](#). His [RH code](#) is now the PRD workhorse.*

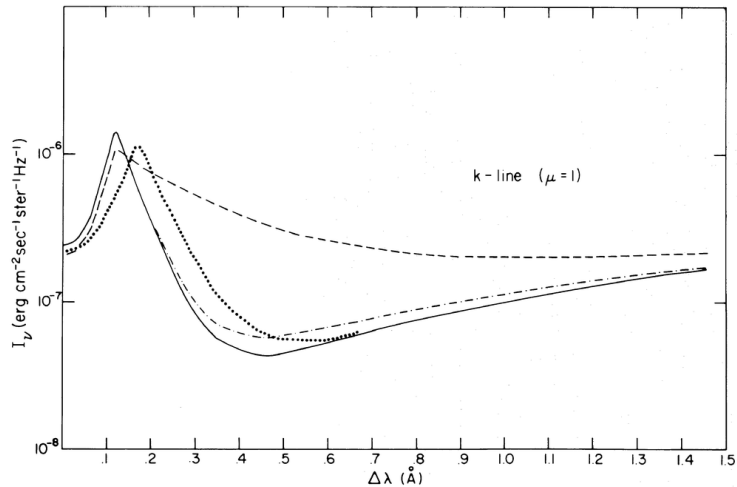


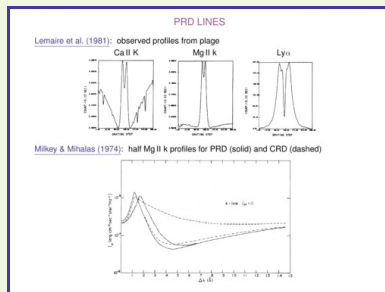
# PRD LINES

Lemaire et al. (1981): observed profiles from plage



Milkey & Mihalas (1974): half Mg II k profiles for PRD (solid) and CRD (dashed)



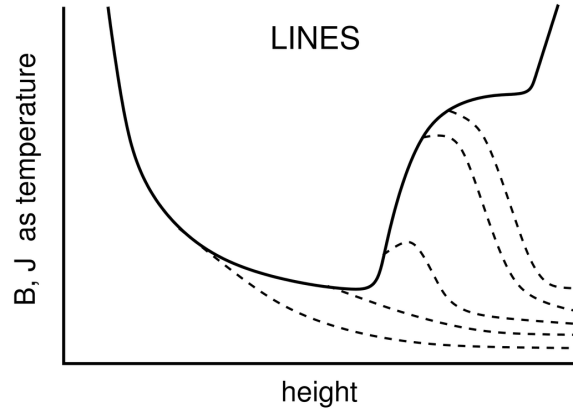
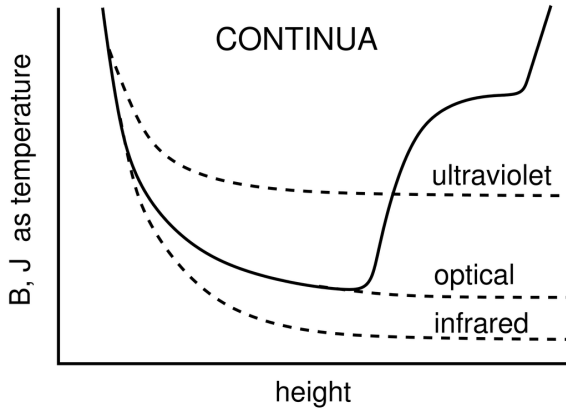


Upper row: classic OSO-8/LPSP observations of plage in the strongest solar resonance lines. The Mg abundance is ten times the Ca abundance. Therefore, the h & k inner wings are formed higher than the H & K inner wings and PRD coherency has much larger effect.

Lower row: classic computational demonstration of the effect of inner-wing coherency in Mg II h & k. The deep dip of the PRD profile (solid, deepest curve) compared to the CRD profile (dashed, flattest curve) demonstrates the effect of independent inner-wing scattering. The other two curves are for PRD with large microturbulence (dotted, affecting the peak wavelength) and with large collisional damping (dot-dashed, affecting the dip intensity).

Note re IRIS: the plage comparison in the upper panels illustrates a major advantage of Mg II h & k to be exploited by IRIS: their inner PRD wings are so dark that any bright feature that gets Doppler-shifted out of the line core will stand out clearly. In particular, the off-limb Ca II H type-II spicules of [De Pontieu et al. \(2007\)](#) are likely to be seen all over the disk in the same fashion as the near-limb Ca II H straws of [Rutten \(2006\)](#), rather than as the on-disk H $\alpha$  absorption-dip RBEs of [Roupe van der Voort et al. \(2009\)](#). With their Dopplershifts dominated by transverse swaying and torsional twisting near the limb and by upward flows with blue-shifted grainy down-the-throat appearance near disk center. [These Ly \$\alpha\$  images](#) from the [VAULT-2 flight](#) indeed show grainy plage, but without Doppler discrimination.

# SUMMARY 1D SCATTERING SOURCE FUNCTIONS

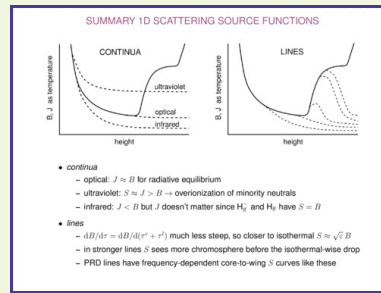


- *continua*

- optical:  $J \approx B$  for radiative equilibrium
- ultraviolet:  $S \approx J > B \rightarrow$  overionization of minority neutrals
- infrared:  $J < B$  but  $J$  doesn't matter since  $H_{\text{ff}}^-$  and  $H_{\text{ff}}$  have  $S = B$

- *lines*

- $\frac{dB}{d\tau} = \frac{dB}{d(\tau^c + \tau^l)}$  much less steep, so closer to isothermal  $S \approx \sqrt{\epsilon} B$
- in stronger lines  $S$  sees more chromosphere before the isothermal-wise drop
- PRD lines have frequency-dependent core-to-wing  $S$  curves like these



Let's recap the effects of 1D scattering on continua and lines.

Cartoons:  $B_{\nu}$  (solid) and  $J_{\nu}$  (dashed) as formal temperature against height for a “typical” solar pixel with a near-radiative-equilibrium photospheric decline, a hump portraying the fibrillar chromosphere, and a thin transition to the corona (likely an extremely warped much-kicked thin-wrap surface).

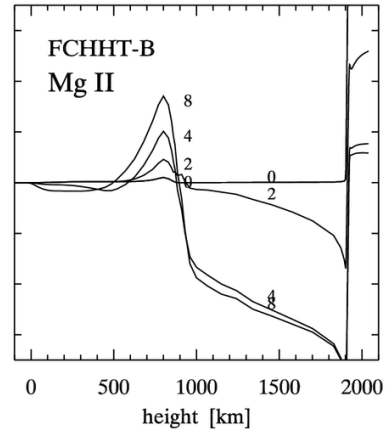
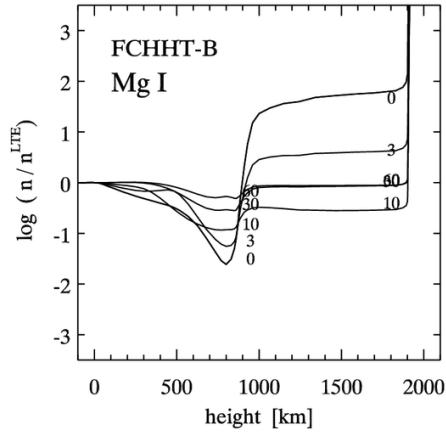
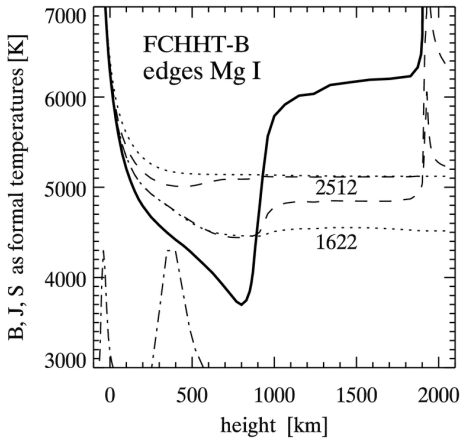
Left: continua. The ultraviolet ones are bound-free scatterers with  $\bar{S}_{\nu} \approx \bar{J}_{\nu} > \bar{B}_{\nu}$ . The bar denotes extinction-weighted frequency averaging over the edge. Complete redistribution holds because each radiative recombination freshly samples the caught-electron Maxwell distribution, without memory of the speed of the freed electron in a previous radiative ionization. Minority species (electron donors Mg I, Fe I, Si I, Al I and alkalis Na I and K I etc.) are overionized in the upper photosphere, so have smaller-than-LTE line opacities. The optical continua (mostly  $H_{\text{b}f}^{-}$ ) have  $S_{\nu} \approx B_{\nu}$ . The infrared continua ( $H_{\text{ff}}^{-}$ ,  $H_{\text{ff}}$ ) have  $S_{\nu} = B_{\nu}$  since free-free interactions are always collisional. However, the  $H_{\text{ff}}^{-}$  opacity can be much out of LTE where hydrogen gets ionized in repetitive shocks and does not recombine quickly in cooler post-shock gas (see below).

Right: lines. Line scattering tends to isothermal-atmosphere behavior because the  $B_{\nu}(\tau_{\nu})$  gradient flattens from adding line opacity. Stronger lines decouple further out. The various curves may also depict independently scattering parts of PRD lines. In these, the effective source function jumps from one to another away from line center. (And to the continuum source function in the outer wings.)

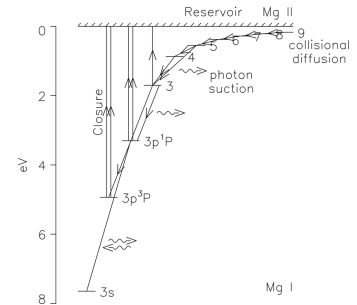
# EXAMPLES: SCATTERING CONTINUA IN A 1D STATIC MODEL

Rutten & Uitenbroek (2012)

FCHHT-B model of [Fontenla et al. \(2009\)](#)



- ultraviolet Mg continua scatter outward from deep photosphere
- photospheric Mg I lines have NLTE opacity depletion
- photospheric Mg II lines have NLTE source function excess
- similar for other electron donors (Si, Fe, Al)



Rutten & Carlsson (1994)

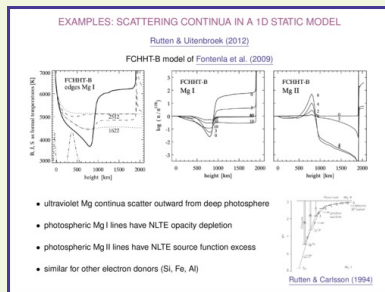


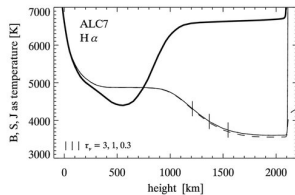
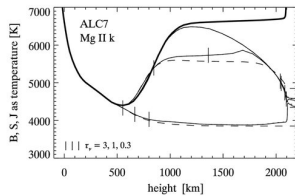
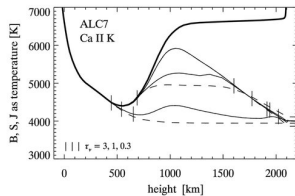
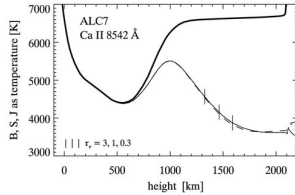
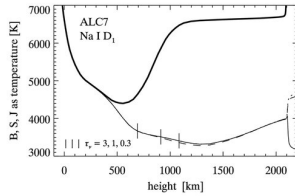
*Illustration: formation of Mg continua and lines in a 1D static model atmosphere. Similar to the classic [VALIIC](#) results and the earlier results for Fe in [Bruce Lites's PhD thesis](#).*

*Mg I has two important ultraviolet edges. The dot-dashed peaks are their intensity contribution functions. Both edges scatter out from the deep photosphere. Their  $J_\nu$  (dotted) does not feel the overlying chromosphere. The 1622 Å edge has slight  $\bar{S} \approx (1 - \epsilon)\bar{J} + \epsilon\bar{B}$  sensitivity to the chromospheric temperature plateau. The more important deeper-formed 2512 Å edge has none.*

*The other two panels show NLTE population departure coefficients  $b_i \equiv n_i/n_i^{\text{LTE}}$  for selected levels (with  $i = 0$  the  $n = 1$  ground state, IDL-wise). In the Wien approximation the line extinction has  $\alpha_\nu^l \approx b_l \alpha_\nu^{\text{LTE}}$ , the line source function  $S_\nu^l \approx (b_u/b_l)B_\nu$ . Thus, lower-level curves define opacity departures from LTE for a given  $l-u$  line transition and divergences between upper- and lower-level curves define line source function departures from LTE. Photospheric Mg I lines typically have lower-than-LTE opacities. Photospheric Mg II lines typically have superthermal source functions.*

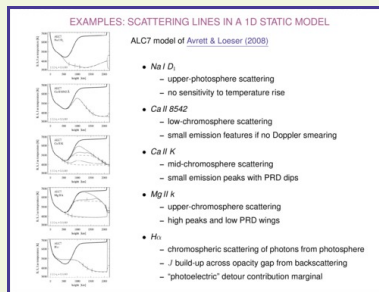
*[Mats Carlsson's](#) ancient cartoon at lower right illustrates major Mg I population mechanisms in the upper photosphere. Most Mg particles are ionized (hence the flat Mg II  $b_0$  curve). A population loop with downward flow through Rydberg levels with Rayleigh-Jeans sensitivity to stimulated emission explains the Mg I 12-micron emission lines ([Carlsson et al. 1992](#)). It is primarily driven by photon losses in upper-photosphere lines. The  $S > B$  imbalance in the 2512 Å edge is the major loop closer.*

# EXAMPLES: SCATTERING LINES IN A 1D STATIC MODEL



## ALC7 model of [Avrett & Loeser \(2008\)](#)

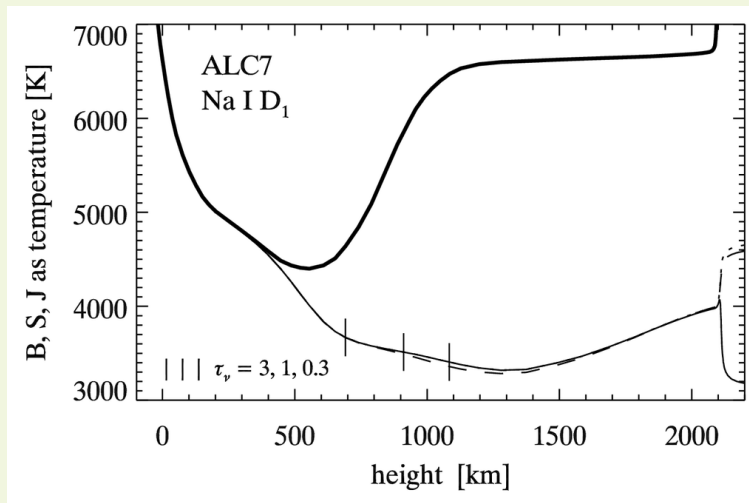
- *Na I D<sub>1</sub>*
  - upper-photosphere scattering
  - no sensitivity to temperature rise
- *Ca II 8542*
  - low-chromosphere scattering
  - small emission features if no Doppler smearing
- *Ca II K*
  - mid-chromosphere scattering
  - small emission peaks with PRD dips
- *Mg II k*
  - upper-chromosphere scattering
  - high peaks and low PRD wings
- *H $\alpha$* 
  - chromospheric scattering of photons from photosphere
  - *J* build-up across opacity gap from backscattering
  - “photoelectric” detour contribution marginal



These graphs are first of all a tribute to Gene Avrett, a giant of solar spectrum theory. At present his productivity is hampered by Rudolph Loeser's pensionership, but [Petr Heinzel](#) and [Michal Herlender](#) now also work with the Pandora code. In my [graduate-level course notes](#) I have elevated the [VALIIC model](#) to stellar status, a didactically magnificent plane-parallel static star that precisely obeys the radiative transfer theory in my notes, developed to no small extent by Gene himself. Of course, my Oslo colleagues and I believe that numerical 3D(t) MHD simulations represent the successor to Pandora and that non-plane-parallelness and dynamism make the solar atmosphere rather more interesting than a plane-parallel static one, and for the chromosphere in particular we think that the fluctuations are the physics, not just minor modulations around a reasonably understood mean. Nevertheless, Gene's modeling has been and remains a beacon in our understanding of solar spectrum formation. And so I use his latest model here for NLTE formation illustration (and regret that I never took portraits of him and Rudolph; I stopped [sticking a camera in your face](#)).

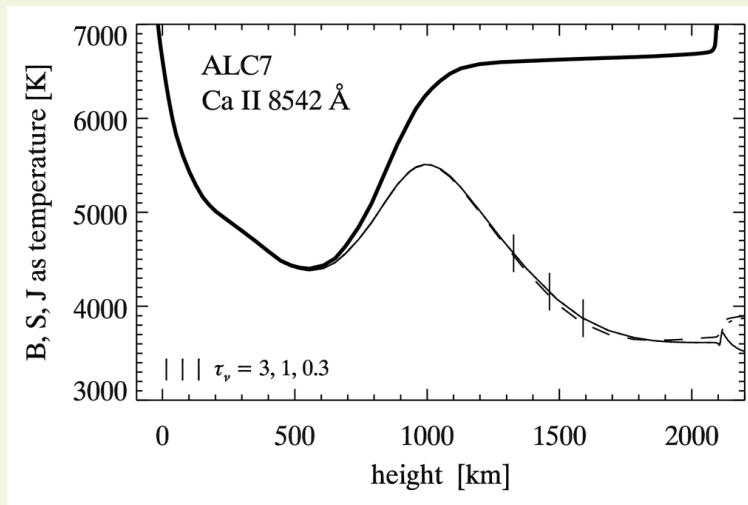
These graphs detail the formation of interesting lines in the ALC7 model (with  $B_\nu$  thick solid, line-center  $S^{\text{total}}$  thin solid,  $\bar{J}_\nu$  dashed and  $S^l$  dotted, all as formal temperatures for easy comparison of different wavelengths). I enlarge and discuss them one-by-one on the following insert displays. I made them with [Han Uitenbroek's RH code](#), including PRD for the lines suffering from it. (Since I managed to run that code, you can too.)





*Na I D<sub>1</sub> is a scattering line closely obeying the  $S^l = (1 - \varepsilon)\bar{J} + \varepsilon B$  CRD two-level law. The source function  $S^{\text{total}} \approx S^l \approx \bar{J}$  drops steeply as for an isothermal atmosphere, decouples well below the ALC7 temperature minimum, and does not sense the ALC7 chromosphere (the slight outward rise is contributed by photospheric continuum  $J_\nu$ ). Most photons escape eventually in the low chromosphere but were created in the low photosphere. Line core Dopplershift or polarization measurement primarily senses the last scatterings and may so sample chromospheric encoding, but for ALC7 the emergent intensity in the line core carries no information on chromospheric temperature.*

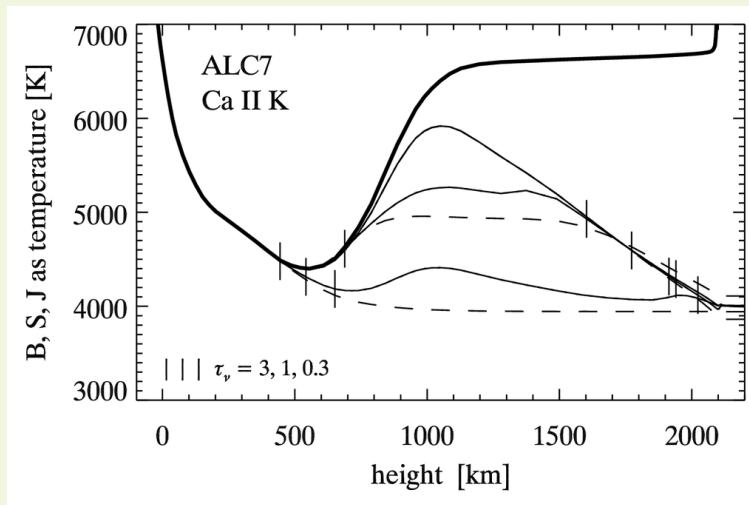
*[Rutten et al. \(2011\)](#) demonstrated that the intensity of the Na I D<sub>1</sub> core is only of minor interest. However, Na I D<sub>1</sub> Dopplergrams turn out to be proxy magnetograms mapping strong-field magnetic elements in the upper photosphere. The reason is that such field concentrations are partially evacuated and harbor magneto-acoustic shocks at lower height than in less magnetic areas. Na I D<sub>1</sub> sees only these deeper shocks. Resonance-cell helioseismology using the Na I D lines is often said to promise chromosphere seismology, but it will rather deliver upper-photosphere magnetic-element seismology.*



The Ca II 8542 Å source function senses the ALC7 chromospheric temperature rise. The resulting source function hump produces tiny emission peaks bordering the deep core in the emergent profile (easily washed out by small-scale motions). The core is dark because it forms in the usual outward scattering decline. Further out than the Na I D<sub>1</sub> core (blink with the previous display), meaning that the ALC7 chromosphere is more opaque in this line.

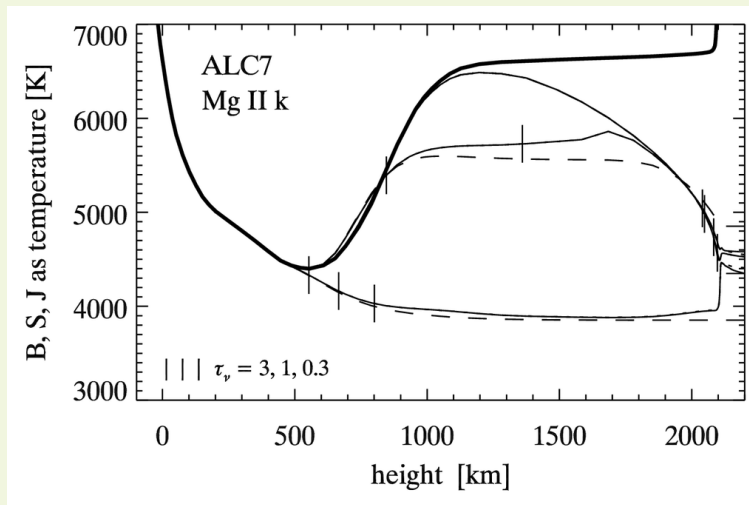
Observationally Ca II 8542 Å indeed shows more chromosphere. Generally the fibrils seen in H $\alpha$  are seen similarly or partially in Ca II 8542 Å while transparent in Na I D<sub>1</sub>. Quiet internetwork cell interiors show the underlying shock-ridden clapotisphere in Ca II 8542 Å ([Vecchio et al. 2009](#)).

Both the 1D static models and the Oslo MHD simulations have difficulty reproducing the profile of this line in spatially-averaged solar atlas data. So it is a promising diagnostic. The core is set by scattering but can show higher intensity at larger temperature ([Cauzzi et al. 2009](#)). It is a well-behaved line with regular opacity stratification. Dopplergrams sense both clapotispheric internetwork shocks and deeper-seated magnetic-concentration shocks ([Rutten et al. 2011](#)).



*Ca II K is a PRD line, so the plot shows source functions at multiple wavelengths. The dashed curves are the monochromatic  $J_\nu$ . The line-center scattering is similar to Ca II 8452 Å but at yet larger opacity. Note the large drop between  $\tau = 1$  and  $\tau = 3$  for the inner-wing source function producing the  $K_2$  peaks. Its  $J_\nu$  drops above  $h = 1500$  km from increasing ALC7 microturbulence. The  $K_3$  dips are formed in the ALC7 temperature minimum without mapping its value. Nothing special, just a fat scattering line. With LTE opacity except where Ca II ionizes. I love it.*

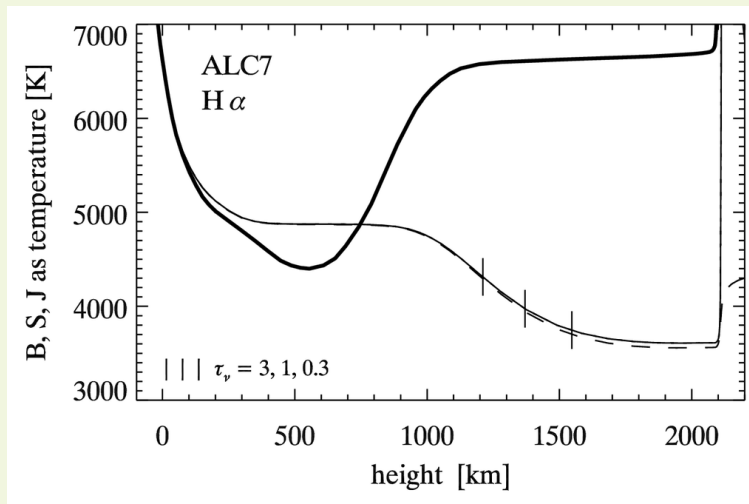
*Observationally, Ca II K should show chromospheric fibrils similar as or thicker than in  $H\alpha$  because Ca II 8542 Å already shows them and H & K have larger opacity. The scattering makes them very dark, however, with low contrast. We don't get too see them (except the very thickest ones in areas with much activity) in DOT or SST or Hinode Ca II H filtergrams because the filter passbands are much too wide. Bright features in the wings beyond the  $K_1$  dips dominate the observed scene. That is why these filtergrams look so similar to TRACE/AIA 1700 Å images of which the internetwork parts are also dominated by clapotispheric acoustics. Ideal for [aligning groundbased data to SDO data](#).*



*Mg II h & k are PRD lines very similar to Ca II H & K, but at 10 times larger elemental abundance (blink with previous display). Chromospheric structures such as  $H\alpha$  fibrils or Ca II H straws/type-II spicules will be much more opaque in h & k and stand out against the PRD-dark inner wings – [as said already](#). IRIS will make us love these lines.*

*In the Mg II Grotrian diagram the triplet lines do not go down from the h & k upper levels as the Ca II infrared lines do, but reach up. (They happen to overlap with h & k in the spectrum.) [Owoccki & Auer \(1980\)](#) showed that h & k are therefore purer scattering lines, with smaller thermalization across small-scale structure, so cleaner density response, than H & K.*

*Other h & k blends provide useful Doppler samplers. The Mn I blends have been invoked in a h & k backradiation pumping mechanism that mistakenly assumed CRD; the photospheric Mn I lines rather derive their unusual activity sensitivity from unusual hyperfine broadening ([Vitas et al. 2009](#)).*

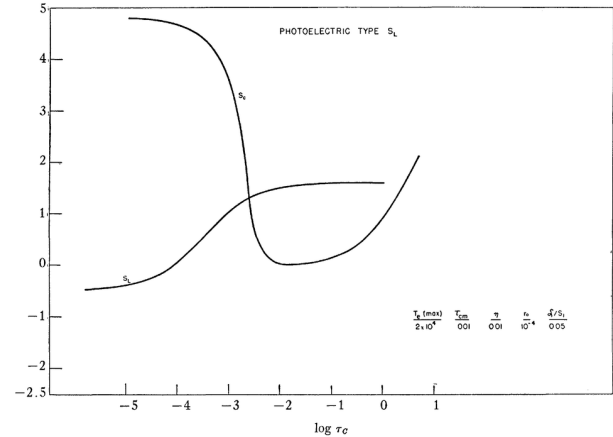
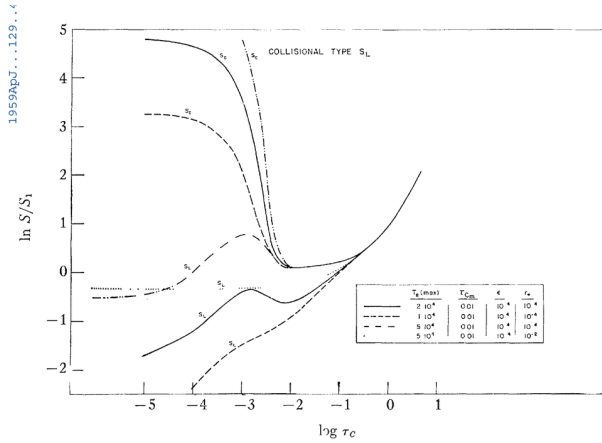


Finally  $H\alpha$ . Blinking against the previous formation diagrams demonstrates that it doesn't display the standard behavior. While the  $H\alpha$  core formation in ALC7 is very similar to that of  $\text{Ca II } 8542 \text{ \AA}$ ,  $H\alpha$  has a flat superthermal source function across the ALC7 temperature minimum that is absent in the other lines.

In a nutshell,  $H\alpha$  has an appreciable opacity gap across the ALC7 temperature minimum. The  $H\alpha$  radiation that is collisionally created in the photosphere scatters across it, hits the heavily scattering ALC7 chromosphere, and some scatters back to raise the value of  $J$  across the gap.

I discuss  $H\alpha$  formation in more detail in the following displays following [Rutten & Uitenbroek \(2012\)](#) and [Leenaarts et al. \(2012\)](#). The first paper uses a static 1D model for didacticism, the latter a 3D(t) MHD simulation snapshot for realism. They are complementary and bring the same message:  $H\alpha$  is foremost a scattering line, with a formation gap between photosphere and chromosphere that enhances its chromospheric signatures. Read on, please. First a return to 1950's theory.

# CANONICAL CHROMOSPHERIC LINE FORMATION

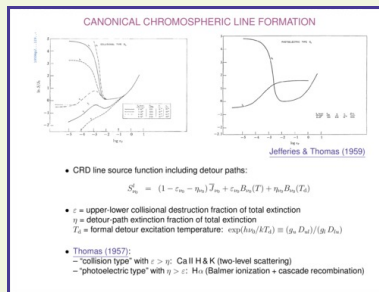


Jefferies & Thomas (1959)

- CRD line source function including detour paths:

$$S_{\nu_0}^l = (1 - \epsilon_{\nu_0} - \eta_{\nu_0}) \bar{J}_{\nu_0} + \epsilon_{\nu_0} B_{\nu_0}(T) + \eta_{\nu_0} B_{\nu_0}(T_d)$$

- $\epsilon$  = upper-lower collisional destruction fraction of total extinction
- $\eta$  = detour-path extinction fraction of total extinction
- $T_d$  = formal detour excitation temperature:  $\exp(h\nu_0/kT_d) \equiv (g_u D_{ul}) / (g_l D_{lu})$
- Thomas (1957):
  - “collision type” with  $\epsilon > \eta$ : Ca II H & K (two-level scattering)
  - “photoelectric type” with  $\eta > \epsilon$ : H $\alpha$  (Balmer ionization + cascade recombination)



Canonical wisdom. The graphs show  $B$  and  $S^l$  against optical depth (outward to the left). Both graphs are reprinted in both the [first \(1970\)](#) and [second \(1978\)](#) editions of Mihalas's "Stellar Atmospheres", the bible of this field. [Jefferies & Thomas \(1959\)](#) produced them to illustrate the classification of [Thomas \(1957\)](#), splitting lines between "collision type" at left and "photoelectric type" at right. They named Ca II H & K an example of the first, H $\alpha$  an example of the latter.

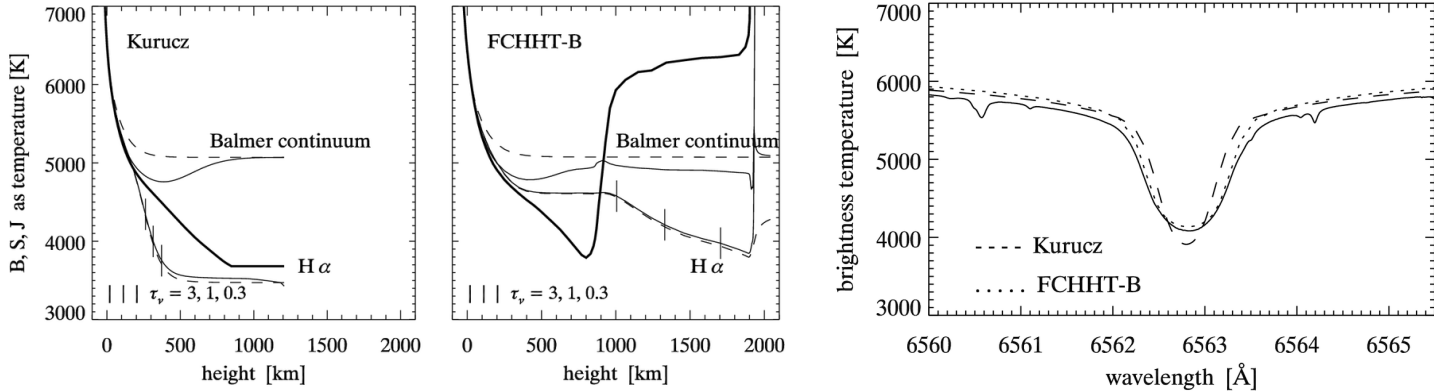
The difference was assigned to the  $\epsilon/\eta$  ratio. For H $\alpha$  the high source function across the upper photosphere in the righthand graph was attributed to preponderance of detour paths, for H $\alpha$  typically Balmer photoionization up from  $n=2$  plus cascade recombination (into high  $n$  followed by downward  $\Delta n=1$  steps) into  $n=3$ .

The lefthand graph is quite similar to my [line-formation cartoon](#) and would indeed explain the ALC7 behavior of [Na I D1](#), [Ca II 8542 Å](#), [Ca II K](#), and [Mg II k](#). The righthand graph is quite similar to the [H \$\alpha\$  ALC7 behavior](#) and should explain that.

So is all well with the canonical wisdom? Not in the ALC7 atmosphere! In this type of model H $\alpha$  is a scattering-dominated line just as the others, with negligible detour contribution except in the transition region. Its unusual superthermal upper-photosphere source function comes instead from chromospheric backscattering across its unusual opacity gap. Read on, please.

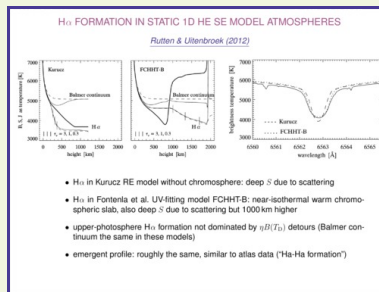
# H $\alpha$ FORMATION IN STATIC 1D HE SE MODEL ATMOSPHERES

*Rutten & Uitenbroek (2012)*



- H $\alpha$  in Kurucz RE model without chromosphere: deep  $S$  due to scattering
- H $\alpha$  in Fontenla et al. UV-fitting model FCHHT-B: near-isothermal warm chromospheric slab, also deep  $S$  due to scattering but 1000 km higher
- upper-photosphere H $\alpha$  formation not dominated by  $\eta B(T_D)$  detours (Balmer continuum the same in these models)
- emergent profile: roughly the same, similar to atlas data (“Ha-Ha formation”)





First graph: H $\alpha$  formation in a Kurucz LTE radiative-equilibrium model without chromosphere. It is a scattering line as Na I D<sub>1</sub> but weaker and formed much deeper.

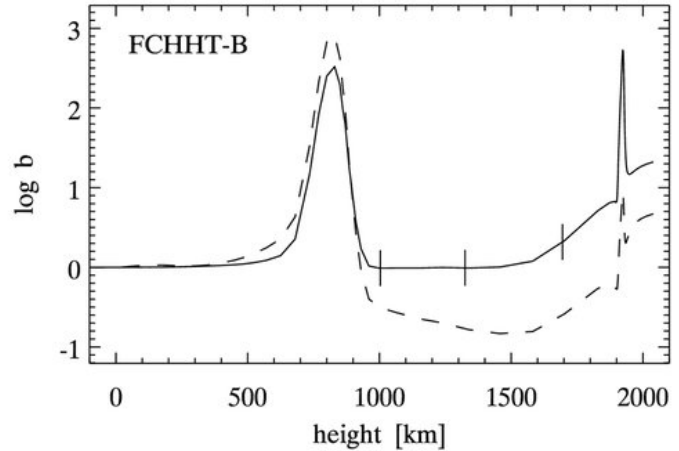
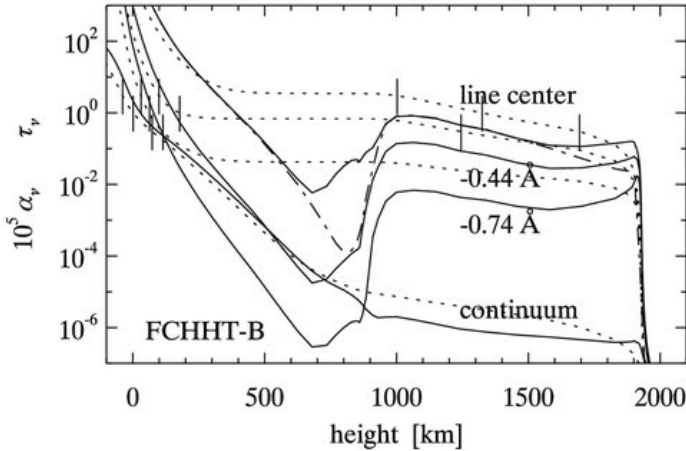
Second graph: H $\alpha$  formation in the 1D static FCHHT-B model of Fontenla et al. (2009). Similar as H $\alpha$  in ALC7, again with high  $S^{\text{total}} \approx \bar{J}$  across the temperature minimum.

These formation curves would be similar if plotted against H $\alpha$  optical depth. The corresponding emergent profiles in the third graph are indeed similar, and fairly close to the disk-center atlas profile (solid). I call this a “Ha-Ha” coincidence because the difference in geometrical terms is enormous: deep-photosphere formation versus high-chromosphere formation. (Corollary: one should never claim reproduction of an observable as proof of a model, and appreciate differences rather than agreement.)

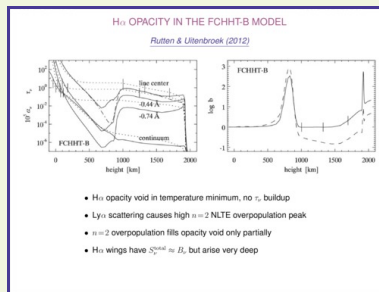
The Balmer continuum  $S$  and  $J$  are overplotted in both formation graphs. They are virtually the same because the two photospheres are virtually the same. Hence, the striking H $\alpha$  differences in  $S$  and  $J$  between the two models have nothing to do with Balmer-continuum detours. Hence, the latter do not cause the superthermal H $\alpha$  source function across the FCHHT-B temperature minimum as suggested in the canonical wisdom.

# H $\alpha$ OPACITY IN THE FCHHT-B MODEL

*Rutten & Uitenbroek (2012)*



- H $\alpha$  opacity void in temperature minimum, no  $\tau_\nu$  buildup
- Ly $\alpha$  scattering causes high  $n=2$  NLTE overpopulation peak
- $n=2$  overpopulation fills opacity void only partially
- H $\alpha$  wings have  $S_\nu^{\text{total}} \approx B_\nu$  but arise very deep



Lefthand graph: H $\alpha$  extinction (solid) and optical depth (dotted) across the FCHHT-B model, at line center, at two wavelengths away from line center, and in the adjacent continuum. The dot-dashed dip is line-center extinction for LTE. The dashes are again  $\tau = 3, 1, 0.3$  marks. The extinction values are multiplied by the chromospheric scale height of 100 km to obtain similar y-scales.

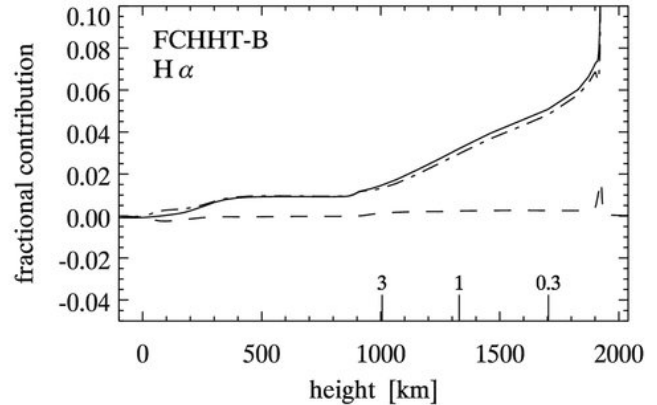
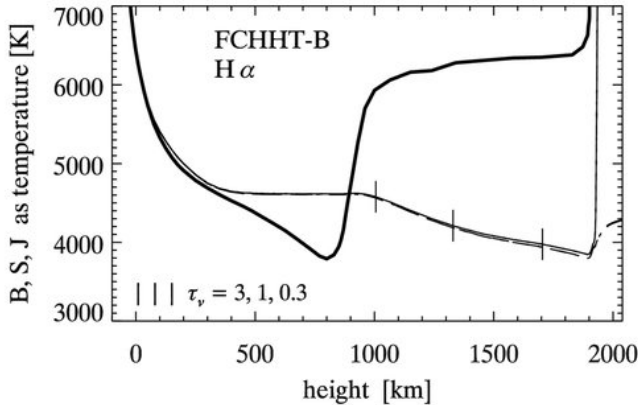
H $\alpha$  has a sizable opacity dip in the temperature minimum due to the high (10 eV) excitation energy of its lower level. It stops the optical depth buildup in this region (plateaus in the dotted curves). H $\alpha$  line center is formed in the chromosphere, which reaches optical thickness  $\tau = 3.5$ . At  $\Delta\lambda = -0.44 \text{ \AA}$  it reaches  $\tau = 0.7$ , at  $\Delta\lambda = -0.74 \text{ \AA}$  only  $\tau = 0.04$ . The outer wings form in the deep photosphere.

Righthand graph: NLTE population departure coefficients for the lower level (solid) and upper level (dashed) of H $\alpha$  in the FCHHT-B model, with line-center  $\tau$  marks. The divergence between the curves corresponds to the  $S-B$  split in the FCHHT-B  $B, S, J$  graph in the [next display](#). The high peak in the lower-level coefficient (which partly fills the LTE opacity dip in the lefthand graph) is caused by scattering in Ly $\alpha$ . This line has  $\bar{S} \approx \bar{J} \approx b_2 B$ . It scatters tremendously, almost everywhere in detailed balance with as many radiative jumps up as down, but the deep sharp temperature minimum of the FCHHT-B model is washed out in its  $\bar{J}$ . The  $b_2$  peak doubles if CRD is assumed for Ly $\alpha$  because core photons can then reach wider via the wings, increasing the smoothing range.

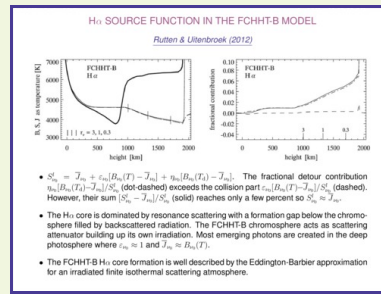
The gentle outward rise of the two curves results from  $J < B$  in the Lyman and Balmer continua.

# H $\alpha$ SOURCE FUNCTION IN THE FCHHT-B MODEL

*Rutten & Uitenbroek (2012)*



- $S_{\nu_0}^l = \bar{J}_{\nu_0} + \varepsilon_{\nu_0}[B_{\nu_0}(T) - \bar{J}_{\nu_0}] + \eta_{\nu_0}[B_{\nu_0}(T_d) - \bar{J}_{\nu_0}]$ . The fractional detour contribution  $\eta_{\nu_0}[B_{\nu_0}(T_d) - \bar{J}_{\nu_0}]/S_{\nu_0}^l$  (dot-dashed) exceeds the collision part  $\varepsilon_{\nu_0}[B_{\nu_0}(T) - \bar{J}_{\nu_0}]/S_{\nu_0}^l$  (dashed). However, their sum  $[S_{\nu_0}^l - \bar{J}_{\nu_0}]/S_{\nu_0}^l$  (solid) reaches only a few percent so  $S_{\nu_0}^l \approx \bar{J}_{\nu_0}$ .
- The H $\alpha$  core is dominated by resonance scattering with a formation gap below the chromosphere filled by backscattered radiation. The FCHHT-B chromosphere acts as scattering attenuator building up its own irradiation. Most emerging photons are created in the deep photosphere where  $\varepsilon_{\nu_0} \approx 1$  and  $\bar{J}_{\nu_0} \approx B_{\nu_0}(T)$ .
- The FCHHT-B H $\alpha$  core formation is well described by the Eddington-Barbier approximation for an irradiated finite isothermal scattering atmosphere.



Lefthand graph:  $H\alpha$   $B$ ,  $S$ ,  $J$  for the FCHHT-B model. Line-center  $S^{\text{total}}$  (thin solid) equals  $\bar{J}$  (dashed) everywhere except in the transition to the corona.

Righthand graph: fractional collisional and detour contributions to the line source function, as specified. The detour contribution becomes dominant in the transition to the corona but that is transparent.

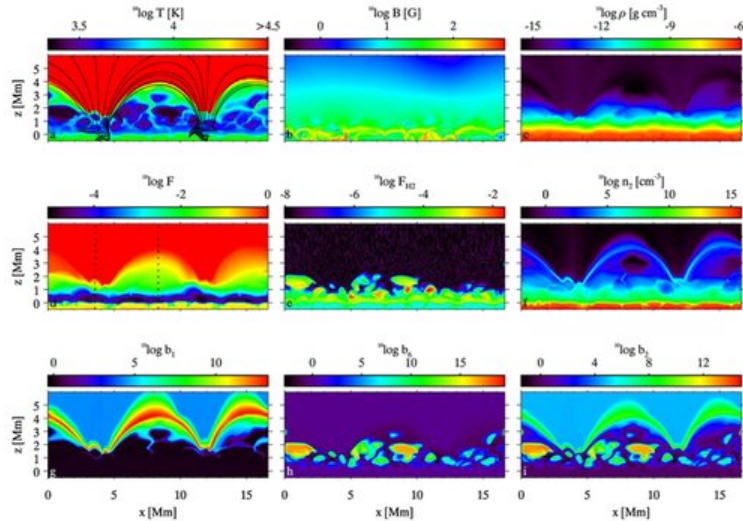
$H\alpha$  is primarily a scattering line, with most photons created in the deep photosphere. Backscattering from the FCHHT-B chromosphere builds up the high  $J$  across the nearly transparent temperature minimum. Corollary: bright shine seen from aside under a dark fibril actually means cool gas there.

Doubling the FCHHT-B chromospheric temperature produces appreciably higher  $S \approx J$ , peaking at 6000 K just above the gap, but also larger  $H\alpha$  opacity so that  $\tau = 1$  is reached already at 1700 km. This further-out sampling of the outward  $J$  decline compensates for the increase, so that  $I(0, 1) \approx S(\tau = 1)$  remains nearly the same. Doubling the chromospheric density produces only 200 K higher  $J$  across the gap, less elsewhere, but also moves  $\tau = 1$  to about 1700 km and so lowers the emergent core intensity appreciably. Upshot: the core intensity is a density rather than a temperature diagnostic. However, the  $H\alpha$  core width is a measure of temperature through the small H atomic mass ([Cauzzi et al. 2009](#)).

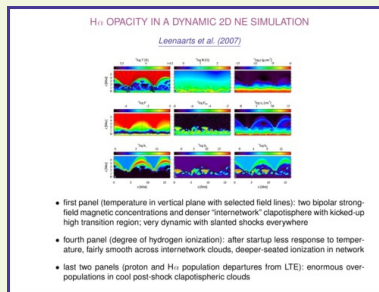
The height extent of the gap equals the width of a full-grown granule. This suggests that 3D scattering smooths the granular scene in the radiation impinging from below on the chromosphere.

# H $\alpha$ OPACITY IN A DYNAMIC 2D NE SIMULATION

*Leenaarts et al. (2007)*



- first panel (temperature in vertical plane with selected field lines): two bipolar strong-field magnetic concentrations and denser “internetwork” clapotisphere with kicked-up high transition region; very dynamic with slanted shocks everywhere
- fourth panel (degree of hydrogen ionization): after startup less response to temperature, fairly smooth across internetwork clouds, deeper-seated ionization in network
- last two panels (proton and H $\alpha$  population departures from LTE): enormous overpopulations in cool post-shock clapotispheric clouds



Movie from [Leenaarts et al. \(2007\)](#). Click on it in the previous display to download and play.

Non-equilibrium (NE) hydrogen ionization/recombination balancing causes much NLTE overionization in cool shocked gas, and similar overexcitation of the ion-slaved  $n = 2$  population defining H $\alpha$  opacity (compare the colorful clouds in the  $b_2$  panel with the  $T$  and  $b_6$  panels). The ion fraction ( $F$  panel) gets much smoother with time. Reason: the collision rate in the 10 eV  $1 \rightarrow 2$  jump is large in hot shocks, small in cool gas ([Carlsson & Stein 2002](#)). The typical three-minute clapotispheric shock repetitivity is too fast to permit hydrogen settling: the next shock kicks the temperature and ionization up again before the neutral fraction comes down to the LTE value for the low post-shock temperature.

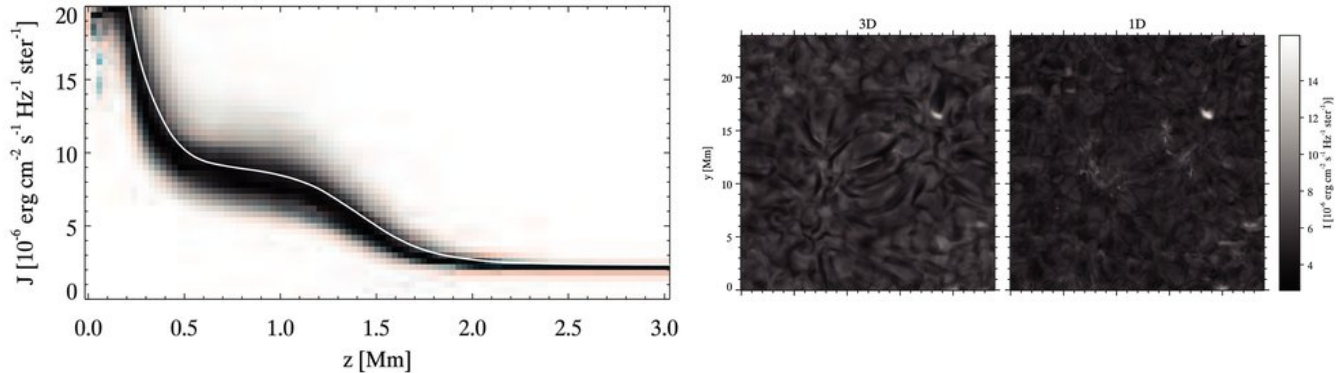
In this simulation spatial Ly $\alpha$  smoothing did not occur because detailed radiative balance was assumed for the Lyman transitions for tractability. The actual smoothing will work the same way as slow recombination, giving larger-than-LTE H $\alpha$  opacity in cool narrow structures from Ly $\alpha$  scattering across them. Also for horizontal ones in 3D.

The high green-yellow-orange arches in the  $b_1$  panel come from cascade recombination where hydrogen ionizes fully. The corresponding arches in the  $n_2$  and  $b_2$  panels are artifacts from the imposed detailed balancing of Ly $\alpha$ .

The  $1 \rightarrow 2$  jump in He I is 20 eV and will similarly affect helium recombination in cooling gas.

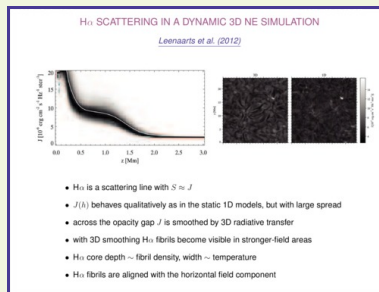
# H $\alpha$ SCATTERING IN A DYNAMIC 3D NE SIMULATION

Leenaarts et al. (2012)



- H $\alpha$  is a scattering line with  $S \approx J$
- $J(h)$  behaves qualitatively as in the static 1D models, but with large spread
- across the opacity gap  $J$  is smoothed by 3D radiative transfer
- with 3D smoothing H $\alpha$  fibrils become visible in stronger-field areas
- H $\alpha$  core depth  $\sim$  fibril density, width  $\sim$  temperature
- H $\alpha$  fibrils are aligned with the horizontal field component



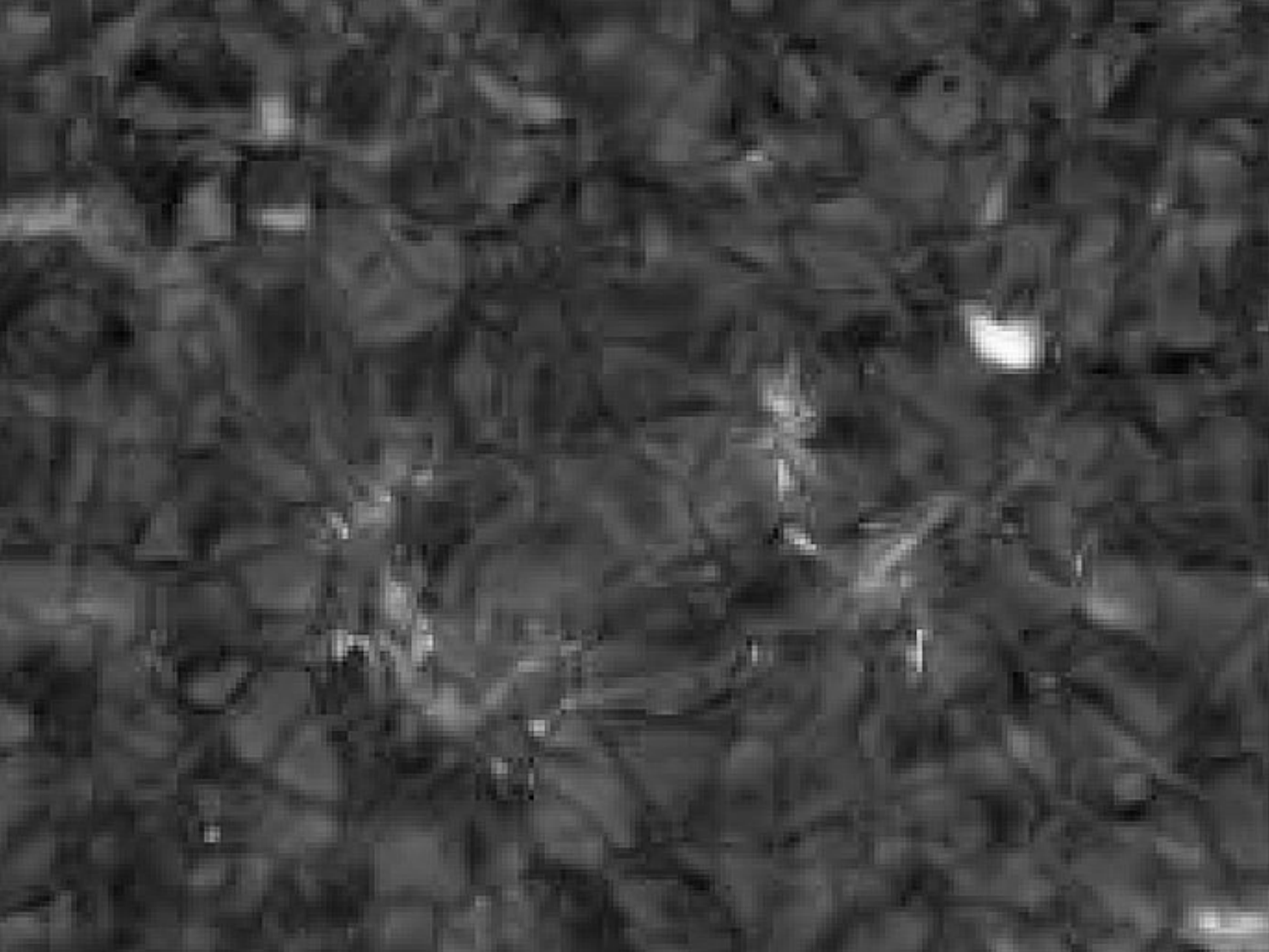


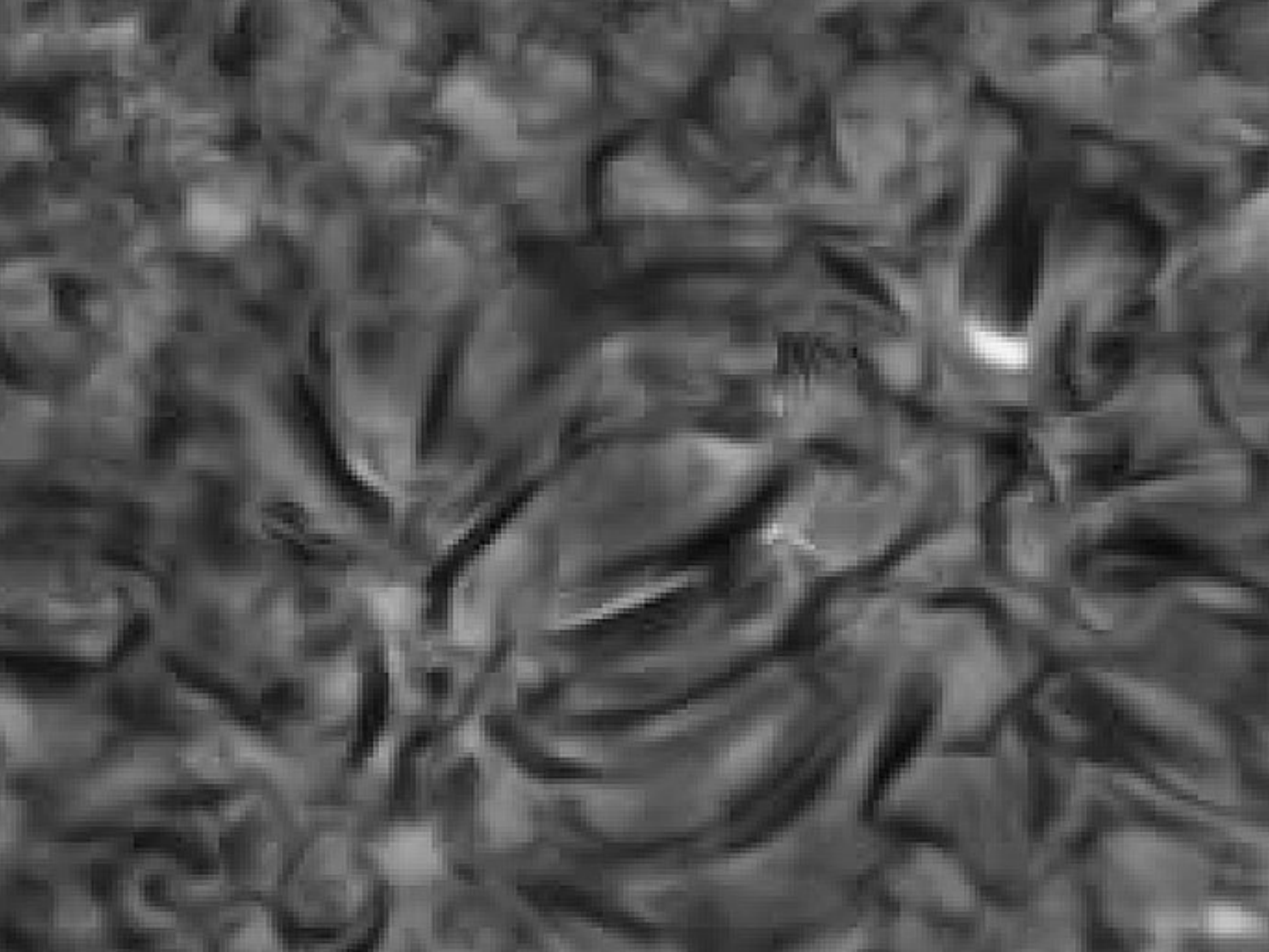
Results from an important recent paper. [Leenaarts et al. \(2012\)](#) used a snapshot from a 3D(t) NE MHD Oslo simulation to synthesize H $\alpha$  with 3D radiative transfer (and some reasonable simplifications).

The lefthand graph shows H $\alpha$   $J_\nu$  behavior similar to the ALC7 and FCHHT-B models: a flat part across the low-opacity upper photosphere filled with scattered and backscattered radiation, followed by an outward scattering decline. The spread is large but the pattern is the same.

The righthand images are two synthesized H $\alpha$  images, in 3D and 1D (line formation computed along vertical columns as if these were 1D plane-parallel stratifications, without knowledge of  $I_\nu$  from other-type columns). I enlarge these images in the next two displays, in reverse order. Blink them and be flabbergasted by the sudden appearance of chromospheric fibrils (in the center where there is more field) in the 3D version! The 3D scattering across the opacity gap obliterates the granular scene imposed in the photosphere and so enhances the visibility of the fibril scene in the chromosphere. The fibrils aren't yet as clear and abundant as in H $\alpha$  observations, but this is their first appearance in an MHD simulation, a triumph.

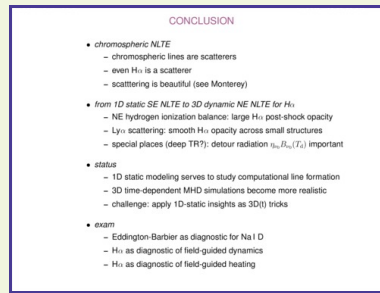
[Leenaarts et al. \(2012\)](#) added displays which confirm that the H $\alpha$  core depth primarily senses density, the core width temperature. In addition, they showed that the fibrils in the 3D image are pretty well aligned with the horizontal component of the magnetic field. Of course, any H $\alpha$  image vividly gives that impression, but it is good to have confirmation of this diagnostic worth.





# CONCLUSION

- *chromospheric NLTE*
  - chromospheric lines are scatterers
  - even  $H\alpha$  is a scatterer
  - scattering is beautiful (see Monterey)
- *from 1D static SE NLTE to 3D dynamic NE NLTE for  $H\alpha$* 
  - NE hydrogen ionization balance: large  $H\alpha$  post-shock opacity
  - $Ly\alpha$  scattering: smooth  $H\alpha$  opacity across small structures
  - special places (deep TR?): detour radiation  $\eta_{\nu_0} B_{\nu_0}(T_d)$  important
- *status*
  - 1D static modeling serves to study computational line formation
  - 3D time-dependent MHD simulations become more realistic
  - challenge: apply 1D-static insights as 3D(t) tricks
- *exam*
  - Eddington-Barbier as diagnostic for Na I D
  - $H\alpha$  as diagnostic of field-guided dynamics
  - $H\alpha$  as diagnostic of field-guided heating



*Scattering was the message in this mini-course. The ultraviolet continua are bound-free scatterers. The chromospheric lines are bound-bound scatterers. Even  $H\alpha$  is primarily scattering and derives its fibril visibility from scattering.*

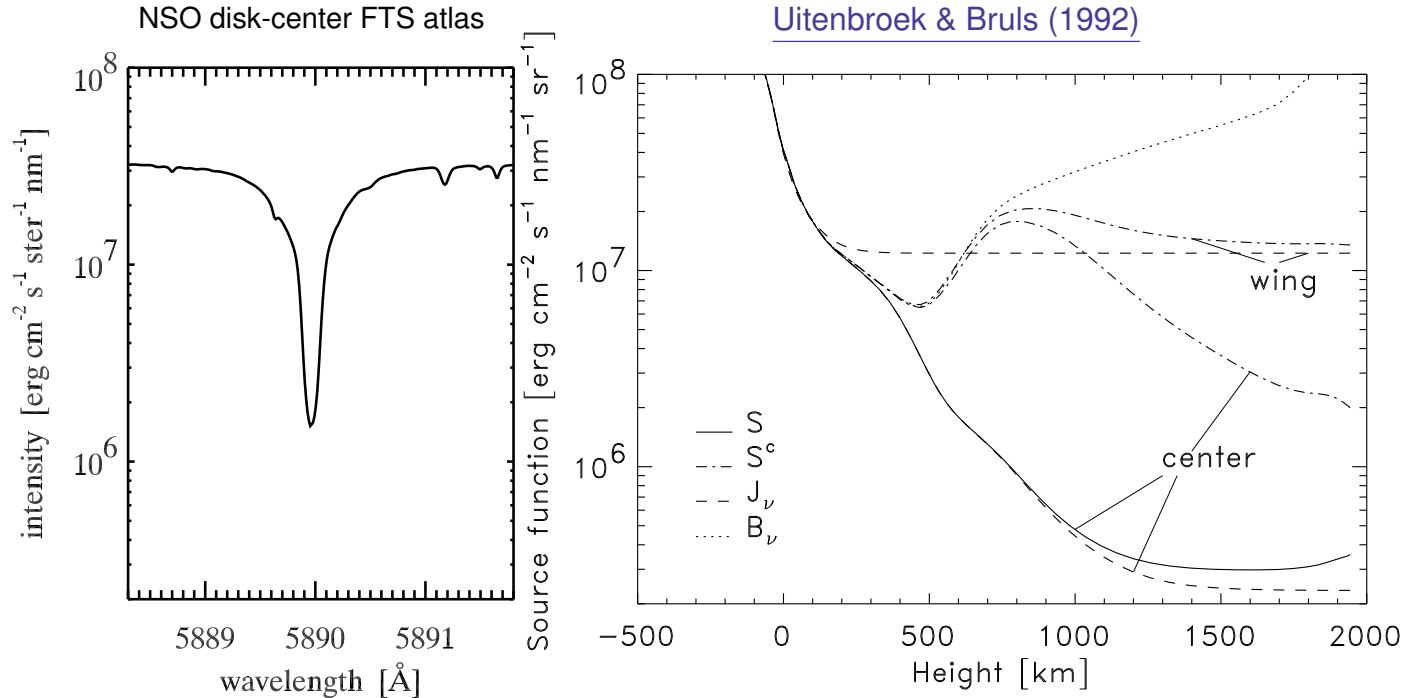
*Scattering is beautiful! Watch the ocean, coast, and sky outside the conference room. This beautiful Monterey vista is all scattered sunlight. If you point a spectroscope at that sea otter in the kelp out there, you get to see all Fraunhofer lines. Including  $H\alpha$ , its core formed in the chromosphere, its wings in the photosphere – while you see it from the sea otter<sup>1</sup>. Even when it is overcast without sun in the sky. Isn't that wonderful?*

*Our prospects are excellent. The simulations are getting realistic even for chromospheric fibrils. IRIS will add Mg II h & k as principal type-II-spicule diagnostics to the comprehensive SDO monitoring. I look forward to IRIS spectrometry of the extreme limb, returning to my original research topic exploiting the extended seeing-free observing that space offers over eclipses. For me this rosy future offsets depressing [Utrecht University stupidity](#) (there were 8 Utrecht alumni here).*

*Time for the exam to this course. Answer the questions at the bottom of the next display.*

<sup>1</sup> *If there were a total eclipse right now the otter would still radiate scattered sunlight containing  $H\alpha$  but without showing the line. Coronal scattering. Beautiful! Bring a sea otter to [Paul's autumn meeting](#)?*

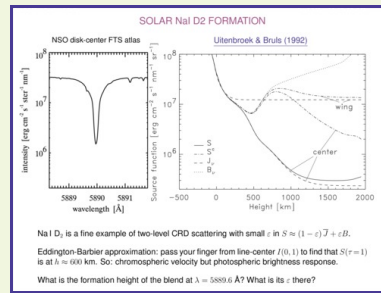
# SOLAR Na I D<sub>2</sub> FORMATION



Na I D<sub>2</sub> is a fine example of two-level CRD scattering with small  $\varepsilon$  in  $S \approx (1 - \varepsilon)\bar{J} + \varepsilon B$ .

Eddington-Barbier approximation: pass your finger from line-center  $I(0, 1)$  to find that  $S(\tau=1)$  is at  $h \approx 600$  km. So: chromospheric velocity but photospheric brightness response.

What is the formation height of the blend at  $\lambda = 5889.6 \text{ \AA}$ ? What is its  $\varepsilon$  there?

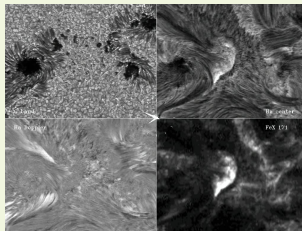


*Gotcha! If you passed your finger from the blend at left to the source function at right, equating the blend intensity at left to the source function  $\approx$  Planck function at right in Eddington-Barbier fashion and so concluded that  $\tau = 1$  lies near  $h \approx 150$  km — then you were a million times wrong. The blend is a telluric line, formed by water molecules in our own atmosphere at (solar) height  $h = 1AU = 150 \times 10^6$  km.*

*Moral: you have to know the identity and nature of your line and understand its formation before you ask me (or Eddington & Barbier) what its formation height is.*

*Cloud modeling is (literally) appropriate for this line, not optically-thick stellar-atmosphere modeling. With  $S_\nu = J_\nu$  and  $\epsilon = 0$  in the cloud.*

*Next exam questions: play [this DOT movie](#). What do you see? Where are the spots? Where is the heat? Why?*



Click on the thumbnail above to download and play the answer movie. If it won't work try the [.mov version](#). The overlay with TRACE 171 Å (lower right) was made by [Alfred de Wijn](#).

The [exam movie](#) (lower-left panel here) shows  $H\alpha$  Dopplergrams at  $\Delta\lambda = \pm 0.5 \text{ \AA}$ . The running penumbal waves are field-guided shocks emanating from umbrae. Even the smallest pores without any discernable penumbra show running penumbral waves in such movies, like the grin of the Cheshire Cat. Their outward expanding field causes these tell-tale spreading Doppler rings.

The  $H\alpha$  core intensity (second panel, [full-frame version](#)) displays many long fibrils and shorter dynamic fibrils. Darker means larger density. Some have bright underneath, meaning cool. The Doppler movie shows lots of fibril oscillations and flows.

Where is the heat? Obviously in the bright patches in  $H\alpha$  core intensity that correspond so closely to the bright one-million Kelvin patches in 171 Å. So-called moss. Greyish in the Doppler movie because large thermal broadening diminishes the Doppler sensitivity. The hot ear-shaped patch left of center is striking. Its large  $H\alpha$  brightness must be large  $\eta B(T_D)$  contribution by cascade recombination. Presumably because the transition to the corona lies very low. But how and why, and why the very sharp extra-bright boundary? A reconnection front in the moat flow? These questions have no answer yet. That's good: something to learn.





**RADIATION FROM ELSEWHERE: THE OPERATOR**

$$J_s(\tau_s) = (1 + \tau_s) \int_0^{\tau_s} I_s d\tau = \int_0^{\tau_s} S_s(\tau_s) E_s(|\tau_s - \tau_s|) d\tau_s = A_s |S_s(\tau_s)|$$

Krieger (1998)

Kourganoff (1952)

**13**

**start index**

The Schwarzschild equation for a plane parallel atmosphere with  $J_s(\tau_s) = \int_0^{\tau_s} e^{-\tau_s(\tau_s - \tau)} d\tau$  defines the *A* operator. This Krieger's graph illustrates its working. Spectrally *S*, Overlap  $E_s(|\tau_s - \tau_s|)$  at the depth of interest  $\tau_s = 0.5$ . Do the multiplication. The fit of *S*( $\tau$ ) produces asymmetry between the two tails. Do the integral (area summation) and divide by 2 to get the mean of the two tail areas. The buffer specifies the resulting  $J_s(0.5)$ . It is below  $S(0.5)$  because the leftward tail is cut at  $\tau = 0$  at the surface whereas the rightward tail continues beyond that point ( $\tau_s = \tau_s$ ). For deeper sampling the result gets closer to *S* because the cut-off part diminishes. Linear *S*( $\tau$ ) therefore produces linear intensity anisotropy (apply Edlén's Beer's law  $S = \tau_s$  around  $\tau_s = 0.5$  and that cancels in the averaging).

If *S*( $\tau$ ) is constant then  $J(0) = 0.5 < S$ . Observe: the Edlén-Berber approximation, exact for linear *S*( $\tau$ ), then says that  $I^{\uparrow}(\mu) = S(\tau) \mu = S$  in any outward direction (Lambert radiators). There is no inward  $I^{\downarrow}$  at the surface, so the angle averaging over all directions gives  $J = S$ . This case is shown in the first Kourganoff graph (with the source function written as *B* for LTE).

When *S*( $\tau$ ) increases steeply inside the rightward tail it wins from the cut-off leftward tail making  $J > S$  near the surface. This is shown in the third Kourganoff graph. The second graph illustrates the radiative-equilibrium gradient  $S = 1 + (3/2) \tau$  producing  $J \approx S$ .

Upshot: steep *S*( $\tau$ ) increases  $J > S$  near the surface, shallow *S*( $\tau$ ) produces  $J < S$  near the surface. With wide-continuum kernels. At larger depth  $J = S$ .

**14**

**THE A OPERATOR FOR AN LTE-RT-RE ATMOSPHERE**

$$J_s(\tau_s) = \int_0^{\tau_s} B_s(\tau_s) E_s(|\tau_s - \tau_s|) d\tau_s = A_s |B_s(\tau_s)|$$

Krieger (1998)

Conversion to formal radiation temperature  $B_s(\tau_s) = J_s$  removes the wavelength-dependence of the Planck function sensitivity to temperature.

**15**

**start index**

The Schwarzschild equation for LTE with  $S_s(\tau) = B_s(T(\tau))$ .

Krieger's plots are for a grey LTE Milne-Edlén atmosphere with solar effective temperature and radiative-equilibrium stratification  $T(\tau) = T_{eff} [1 + (3/2)\tau]^{2/3}$ . The upper plots show  $B_s$  and  $J_s$  against depth, the lower plots the corresponding formal temperatures. The latter are better suited for the different wavelength comparison by sharing the same x-axis extent.

Since the bulk of the flux comes out in the visual the center panels have  $\mu = 0.6$  to produce the spectrum-wide  $J_s^{\uparrow}(\mu) = (S_s - J_s) \mu$  radiative-equilibrium condition.

At short wavelengths the larger Wien response of the Planck function to temperature causes steeper  $B_s(\tau)$  increase and therefore  $J_s = B_s$ . Note the large y-axis range at the upper-left panel.

At long wavelengths the Planck function has only linear Rayleigh-Jeans sensitivity to the temperature so that the  $B_s(\tau)$  gradient is much less steep, resulting in  $J_s < B_s$ .

Upshot: upper photographs continue  $J_s = B_s$  at short wavelengths,  $J_s < B_s$  at long wavelengths, already in the absence of scattering.

**16**

**SCATTERING IN AN ISOTHERMAL CONSTANT-EPSILON ATMOSPHERE**

$$J_s(\tau_s) = A_s |S_s(\tau_s)| \quad S_s' = (1 - \epsilon_s) J_s + \epsilon_s B_s$$

Arndt (1965)

- "dark" fog:  $S(0) = \sqrt{B}$
- Gaussian line in CRD:  $S = B$  (thermalization at depth  $\tau = 1$ )
- damping wings in CRD: deeper thermalization from photon escape in wings

**17**

**start index**

The Schwarzschild and two-level-scattering equations together govern the behavior of *S* and *J*. Aron's classic graphs are for an isothermal homogeneous two-level atom gas with constant collisional photon destruction probability per extinction - assuming complete redistribution (CRD) - no coherency = no monochromatic scattering of photons; more below.

For LTE = 1,  $S(0) = B + 1$ ,  $J(0) = 0.5 S$ . The surface is a half-isotropic Lambert radiator.

For smaller  $\epsilon$  the surface value  $S(0)$  goes down following the  $\sqrt{\epsilon}$  law. The emergent intensity  $J(0) = S(0) \mu = 1$  becomes very busy, about  $\sqrt{\epsilon} J$ . As a fig. showing the thermalization height. If you add a layer to the atmosphere  $\epsilon$  will scatter photons back without creating as many new ones.

In deep layers the radiation field isn't aware yet that photons can escape. There the radiation field is only linearly anisotropic with  $J = B$ . In a real atmosphere with density stratification  $\epsilon = 1$  with depth as the collision frequency increases. Both  $S$  and  $J$  with depth.

At more scattering the knowledge that there is an escape surface propagates inward. The "thermalization depth" where  $S = B$  is at  $\tau = 1/\epsilon$  for CRD and constant  $\epsilon$ . If the line has damping wings the thermalization depens further (rightward plot) because photons have larger escape probability in the extended low- $\epsilon$  wings.

Upshot: scattering darkens the emergent intensity and deepens the thermalization tremendously.

**18**

**SCATTERING IN EPSILON = 0.01 ATMOSPHERES**

$$J_s(\tau_s) = A_s |S_s(\tau_s)| \quad S_s' = (1 - \epsilon_s) J_s + \epsilon_s B_s$$

Krieger (1998)

**19**

**start index**

Again the Schwarzschild and two-level-scattering equations, one for coherent scattering (see last on *J*). Again two-level-atom gas, with depth-independent destruction probability  $\epsilon = 10^{-2}$ . *B*, *S*, *J* curves against depth (solid, dashed, dotted). Diamonds and crosses, *J* and *S* from the Edlén approximation which assumes linearly anisotropic intensity. It is pretty good.

Upper row: linear *B*( $\tau$ ) isothermal. The first panel for the isothermal case is similar to the  $\epsilon = 10^{-2}$  curve of Arndt's graph, except that thermalization occurs at  $\tau = 1/\epsilon$  because here coherent (monochromatic) scattering is assumed. The second panel has the radiative-equilibrium gradient producing  $S = B$ . The third panel has a step-Planck-function gradient, also with thermalization at  $\tau = 1/\epsilon$ , but has no evident because all three curves drop steeply.

Lower row: sort-of-solar temperature stratification with a radiative-equilibrium photosphere, a flat temperature minimum, and a photospheric temperature rise. Parameter  $\epsilon$  is the line-to-continuum extinction ratio ( $\epsilon'$ ) also assumed depth-independent. For stronger lines *J* and *S* decrease further out from *B*. In each case they drop away from that point. For this rather large  $\epsilon$  the source function still senses the chromospheric temperature.

Strong lines do not have  $J = B$  even at short wavelengths where continuum do, because their gradient  $dS/d\tau = dS'/d\tau + \epsilon S = dS/(1 + \epsilon S)$  is much less steep than  $dS/d\tau$ . Strong lines therefore tend to the isothermal case.

**20**

**FREQUENCY COHERENCE OR REDISTRIBUTION**

- Edlénizing: does a emitting atom remember at which frequency it was excited?
- coherent scattering: incoming and outgoing photons have the same frequency
- Doppler redistribution: coherent scattering in atom frame. Doppler shifts in observer frame
- collisional redistribution: reshuffling while the atom sits in the upper state
- complete redistribution: no memory but a fresh sample of the probability distribution
- coherent scattering in different parts of a spectral line:

**21**

**start index**

Curious: resonance scattering into the beam for a transition with a sharp (infinite lifetime) lower level. The upper level may be regarded as widened against the extinction profile. In coherent (monochromatic) scattering the outgoing photon has precisely the same frequency as the incoming one. Its complete redistribution (CRD) the outgoing photon samples the profile function. Doppler redistribution occurs over the Doppler width in the frame of the observer for coherent scattering in the frame of the atom. Systemic motion may upset this Maxwellian ensemble notion, making addition of "line-of-sight" even more suspect than it already is.

Collisional redistribution may be described as a resonant phase jump from abrupt encounters in the impact approximation, or a term-dipgram resulting from successive neighbor changes in the quasi-static approximation. Obviously more important at larger collisional/density density. Hence deeper in the atmosphere.

Graphs: the same as on the previous task. Note they are interpreted as illustrating the effects of coherent scattering in the core, line, and outer wing of a strong line. Each part of the line has its own monochromatic thermalization depth and its own corresponding frequency-dependent source function behavior.

**22**

**PARTIAL REDISTRIBUTION**

Mihalas (1978) chapter 13

- Doppler redistribution over the Dopplerwidth in the frame of the observer
- collisional damping: redistribution
- formation of a line strong enough that radiation damping dominates in the inner wings (high formation to low collisionality theory):
- the core source function is only Doppler redistribution
- the inner wings have nonresonant line source functions with Dopplerwidth smearing
- the outer wings are collisional redistributed approximately in CRD
- the inner-wing line source functions decouple deeper from the Planck function than the core source function due to the smaller opacity (each represents a weaker line)
- the PRD core source function decouples further out than for complete redistribution in which core photons can escape already from deeper layers via the wings

**23**

**start index**

Left-hand curves: partial coherency across the extinction profile. Doppler redistribution occurs in the frame of the observer for coherent scattering in the frame of the atom. It causes redistribution over the Doppler core. The outer wings are usually formed so deep in the atmosphere that the large collision frequency for nearest neighbor density here causes collisional redistribution. The inner wings, when dominated by natural damping (Eddington uncertainty principle), scatter coherently, again with Doppler redistribution in the observer.

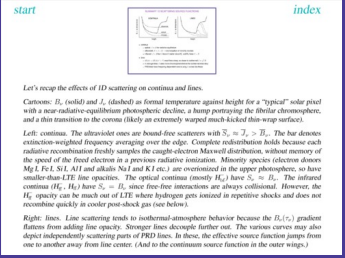
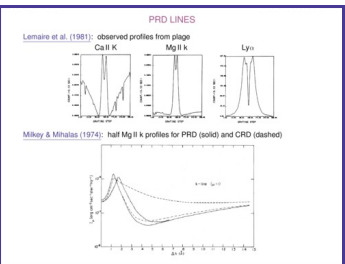
Right-hand curves: the PRD Doppler core, inner wing parts, and the outer wings represent independent photon ensembles. Each scatters outwards in its own manner, each with its source function decoupling from the Planck function at its own thermalization height. With deeper decoupling and escape further into the wings.

The CRD core source function represents a sort of frequency average over the whole profile and so decouples higher than the PRD wings, lower than the PRD core.

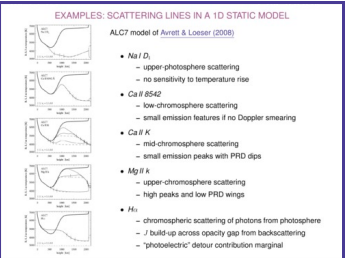
Personal note: my senior thesis (Krieger) wrote a famous (since 1942) about complete redistribution in Fraunhofer lines. He took me to three solar eclipses; the third provided by him; material on coherency in B&B 454. My first graduate student, Hans (Krieger), added core-redistribution between C II H & B and the C II IR lines in his thesis. His B&B code is now the PRD workhorse.

**24**

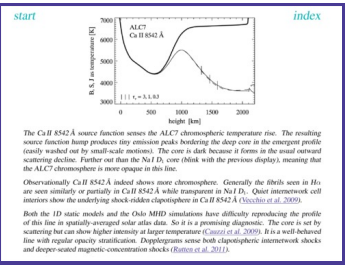
25



28

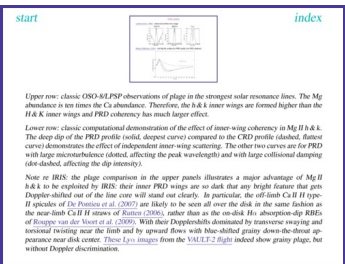


31

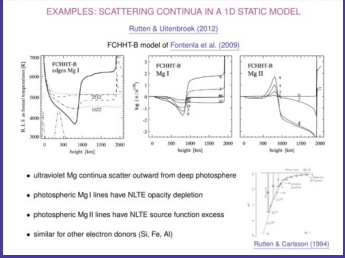


34

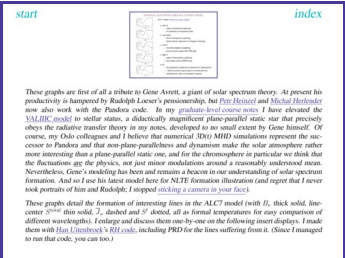
start



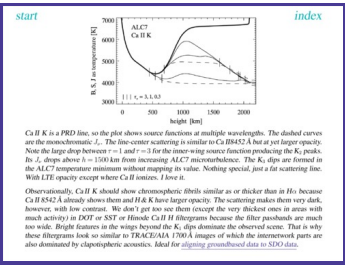
29



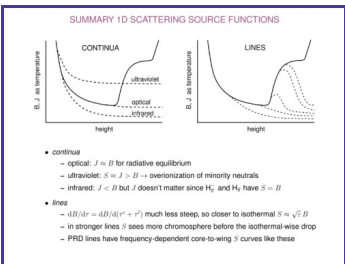
32



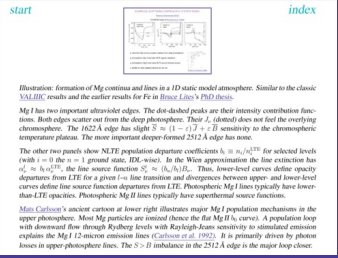
35



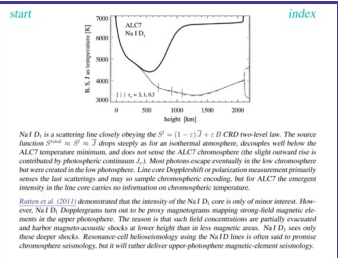
index



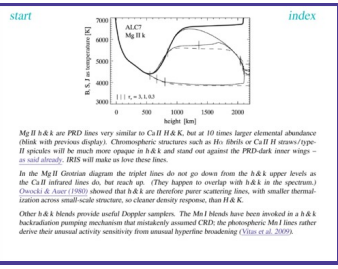
27



30



33



36

**start** **index**

Finally **H<sub>1</sub>**: Blanking against the previous formation diagrams demonstrates that it doesn't display the standard behavior. While the **H<sub>1</sub>** core formation in ALCT is very similar to that of Ca II H&K, **H<sub>1</sub>** has a flat upper photosphere source function across the ALCT temperature minimum that is absent in the other lines.

It is unhelpful. **H<sub>1</sub>** has an appreciable opacity gap across the ALCT temperature minimum. The formation region is collimated center to the photosphere scatterers across it. It is the heavily scattering ALCT chromosphere; and some scatterers back to raise the value of  $\tau_{0,0}$  across the gap.

It doesn't **H<sub>1</sub>** formation in more detail at the following slides following Evers & Ulmer (2012) and Lecarron et al. (2012). The first paper uses a static 1D model for detection, the latter a 3D MHD simulation supported for future. They are complementary and bring the same message: **H<sub>1</sub>** is formed as scattering line, with formation gap between chromosphere and chromosphere that enhances its chromospheric signature. Read on page. First a return to 1980's theory.

**37**

**start** **index**

CANONICAL CHROMOSPHERIC LINE FORMATION

Jaffrés & Thomas (1959)

- CRD line source function including detour paths:
 
$$S_{\nu} = (1 - \tau_{\nu} - \kappa_{\nu})T_{\nu} + \kappa_{\nu}B_{\nu}(T_{\nu})$$
- $\tau_{\nu}$  = upper-lower collisional destruction fraction of total extinction  
 $\kappa_{\nu}$  = detour-path extinction fraction of total extinction  
 $T_{\nu}$  = formal detector temperature:  $\kappa_{\nu}B_{\nu}(T_{\nu}) = (\kappa_{\nu}D_{\nu})/(\mu_{\nu}D_{\nu})$
- Thomas (1957):  
 - "topline type" with  $\tau > \kappa$ : Ca II H&K two-level scattering  
 - "photoelectric type" with  $\tau < \kappa$ : H<sub>1</sub> (Balmer ionization + cascade recombination)

**38**

**start** **index**

Canonical wisdom: The graphs above **H** and **S'** against optical depth (read to the left). Both graphs are repeated in both the first (1970) and second (1973) editions of Milhaud's "Solar Atmosphere", the bible of the field. Jaffrés & Thomas (1959) produced an alternate classification of Thomas (1957), splitting lines between "collision type" at 400 and "photoelectric type" of light. They named Ca II H&K an example of the first. **H<sub>1</sub>** an example of the latter.

The difference was assigned to the  $\tau/\kappa$  ratio. For **H<sub>1</sub>** the high source function across the upper photosphere in the right-hand graph was attributed by reponderance of detour paths. For **H<sub>1</sub>** typically Balmer photoionization up from  $n=2$  plus cascade recombination (into high  $\nu$ , followed by downward  $\Delta n=1$  steps into  $n=2$ ).

The left-hand graph is quite similar to my line-formation code and would indeed explain the ALCT behavior of  $S_{\nu}(D_{\nu}, \chi_{\nu})/S_{\nu}(S_{\nu}, \chi_{\nu})$ ,  $C_{\nu} I_{\nu}$  and  $M_{\nu} I_{\nu}$ . The right-hand graph is quite similar to the **H<sub>1</sub>** ALCT behavior of  $S_{\nu}(D_{\nu}, \chi_{\nu})/S_{\nu}(S_{\nu}, \chi_{\nu})$ .

So is it all about the canonical wisdom? Not in the ALCT atmosphere! In this type of model **H<sub>1</sub>** is a scattering-dominated line just as the others, with negligible detour contribution except in the transition region. Its unusual superphotosal upper photosphere source function comes instead from chromospheric backscattering across its unusual opacity gap. Read on, please.

**39**

**H<sub>1</sub> FORMATION IN STATIC 1D BE SE MODEL ATMOSPHERES**

Rutten & Ulmer (2012)

- H<sub>1</sub>** in Kurucz RE model without chromosphere: deep  $\nu$  due to scattering
- H<sub>1</sub>** in Fontana et al. UV-fitting model FCHFT-B: near-isothermal warm chromosphere, little deep  $\nu$ , height of formation  $\sim 1000$  km higher
- upper photosphere **H<sub>1</sub>** formation not dominated by  $\mu(T_{\nu})$  detours (Balmer continuum the same in these models)
- emergent profile: roughly the same, similar to atlas data ("H $\alpha$ -H $\alpha$  format")

**40**

**start** **index**

First graph: **H<sub>1</sub>** formation in a Kurucz LTE radiative-equilibrium model without chromosphere. It is a scattering line as  $S_{\nu}(D_{\nu}, \chi_{\nu})$  but weaker and formed much deeper.

Second graph: **H<sub>1</sub>** formation in the 1D static FCHFT-B model of Fontana et al. (2009). Similar as **H<sub>1</sub>** in ALCT, again with high  $S_{\nu}(D_{\nu}, \chi_{\nu})$  across the temperature minimum.

These formation curves would be similar if plotted against **H<sub>1</sub>** optical depth. The corresponding emergent profiles in the third graph are indeed similar, and fairly close to the disk-center atlas profile (middle). I call this "1D H $\alpha$  look-alike" because the difference is a generalized semi-incoherent deep-photosphere formation versus high-photosphere formation. Caution: one should never claim reproduction of an observable as proof of a model, and approximate differences rather than agreement!

The Balmer continuum and  $\mu$  and  $\mu$  against formation graphs. They are virtually the same because the two photospheres are virtually the same. Hence, the striking **H<sub>1</sub>** differences in **S** and **J** between the two models have nothing to do with Balmer continuum detours. Hence, the later do not cause the spectral **H<sub>1</sub>** source function across the FCHFT-B temperature minimum as suggested in the canonical wisdom.

**41**

**H<sub>1</sub> OPACITY IN THE FCHFT-B MODEL**

Rutten & Ulmer (2012)

- H<sub>1</sub>** opacity void in temperature minimum, not  $\nu$  buildup
- $\nu$  scattering causes high  $\nu$  = NLTE overpopulation peak
- $\nu$  = 2 overpopulation **H<sub>1</sub>** opacity void only partially
- H<sub>1</sub>** wings have  $S_{\nu}^{\text{obs}} \approx I_{\nu}$ , but arise very deep

**42**

**start** **index**

Left-hand graph: **H<sub>1</sub>** extinction (solid) and optical depth (dashed) across the FCHFT-B model, at line center, at two wavelengths away from line center, and in the adjacent continuum. The dot-dashed dip in line-center extinction for LTE. The dashes are again  $\tau_{\nu} = \chi_{\nu} I_{\nu} / \Omega$  marks. The extinction values are multiplied by the chromospheric scale height of 100 km to obtain similar  $\tau$  scales.

**H<sub>1</sub>** has a sizable opacity dip in the temperature minimum due to high (10eV) excitation energy of its lower level. It tops the optical depth buildup in this region (plotted in the dotted curves). Its line center is formed in the chromosphere, which reaches optical thickness  $\tau = 3.5$ . At  $\Delta\lambda = -4.14$  Å it reaches  $\tau = 0.7$ , at  $\Delta\lambda = -0.74$  Å only  $\tau = 0.04$ . The outer wings are thin in the deep photosphere.

Right-hand graph: NLTE radiation transport coefficients for the lower level (solid) and upper level (dashed) of **H<sub>1</sub>** in the FCHFT-B model, with line center  $\tau$  marks. The divergence between the curves corresponds to the  $S$ - $\nu$  split in the FCHFT-B  $S_{\nu}$  graph in the next slide. The high peak in the lower level coefficient is due to the LTE opacity dip in the left-hand graph is caused by scattering in  $\nu$ . This line has  $S = \nu = J = I_{\nu}$ . **H<sub>1</sub>** scatters reemissions, almost everywhere in detailed balance with a many radiative jumps up to  $\nu$ , but the deep sharp temperature minimum of the FCHFT-B model is washed out as in  $\nu$ . The  $I_{\nu}$  peak doubles if CRD is assumed for  $I_{\nu}$  because one photon can then reach twice up to the wings, increasing the scattering angle.

The gentle  $\nu$ -side dip of the  $\nu$  curves results from  $J < I_{\nu}$  in the Evers and Balmer continua.

**43**

**H<sub>1</sub> SOURCE FUNCTION IN THE FCHFT-B MODEL**

Rutten & Ulmer (2012)

- $S_{\nu} = \tau_{\nu} S_{\nu} + (1 - \tau_{\nu} - \kappa_{\nu})T_{\nu} + \kappa_{\nu}B_{\nu}(T_{\nu})$  (dotted-dashed) encodes the collision part  $(1 - \tau_{\nu})T_{\nu}$  distribution. However, their sum  $S_{\nu} = \tau_{\nu} S_{\nu} + (1 - \tau_{\nu} - \kappa_{\nu})T_{\nu} + \kappa_{\nu}B_{\nu}(T_{\nu})$  reaches only a few percent  $S_{\nu} \approx \tau_{\nu} S_{\nu}$ .
- The **H<sub>1</sub>** core is dominated by resonance scattering with a formation gap below the chromosphere filled by backscattered radiation. The FCHFT-B chromosphere acts as scattering alternator building up its own irradiation. Most emergent photons are created in the deep photosphere where  $\tau_{\nu} = 1$  and  $\mu_{\nu} \approx \mu(T_{\nu})$ .
- The FCHFT-B **H<sub>1</sub>** core formation is well described by the Eddington-Balmer approximation for an irradiated finite isothermal scattering atmosphere.

**44**

**start** **index**

Left-hand graph: **H<sub>1</sub>**, **S**,  $\nu$ ,  $J$  for the FCHFT-B model. Line-center  $S_{\nu}^{\text{obs}}$  (this solid equals  $J$ ) (dotted) where except in the transition is the core.

Right-hand graph: fractional collisional and detour contributions to the line source function, as expected. The detour contribution becomes dominant in the transition to the core but that is transparent. **H<sub>1</sub>** is primarily a scattering line, with most photons created in the deep photosphere. Backscattering from the FCHFT-B chromosphere builds up the high  $J$  across the nearly transparent temperature minimum. Conclude: high- $\nu$  lines come from much under a dark (but actually) mean cool gas phase.

Disabling the FCHFT-B chromosphere's temperature produces appreciably higher  $S_{\nu}$ ,  $J$ , peaking at 6000 K above the gap, but also larger **H<sub>1</sub>** opacity so that  $\tau = 1$  is reached already at 1700 km. This further cut sampling of the coronal  $\nu$  declines temperature as temperature increases.  $\nu$  is nearly unity near the core. Disabling the chromospheric density produces only 20% higher  $J$  across the gap, but also  $\nu = 1$  at about 1700 km and a lower and the emergent core intensity accordingly. Embellish the core intensity a density below a temperature diagnostic. However, the **H<sub>1</sub>** core width is a measure of temperature through the small **H** atomic mass (Lecarron et al., 2009).

The high extent of the gap equals the width of a full photosphere. This suggests that 3D scattering smooths the granular scale in the radiation impinging from below on the chromosphere.

**45**

**H<sub>1</sub> OPACITY IN A DYNAMIC 2D NE SIMULATION**

Lecarron et al. (2007)

- first panel (temperature in vertical plane with selected field lines): two bipolar strong-field magnetic concentration/detour configurations with high- $\nu$  transition region; very dynamic with slanted shock everywhere
- fourth panel (degree of hydrogen ionization): after startup less response to temperature, fairly smooth across internetwork clouds, deeper-seated ionization in network
- last two panels (iron and **H<sub>1</sub>** population diagnostics from LTE): enormous overpopulation in cool post-shock chromospheric regions

**46**

**start** **index**

Movie from Lecarron et al. (2007). Click on it in the previous slide to download and play.

Non-equilibrium (NE) hydrogen ionization/recombination balancing causes much NLTE overionization in cool shocked gas, and similar overionization of the ion-slaved  $\nu = 2$  population diverting **H<sub>1</sub>** opacity (compare the colored clouds in the  $\nu$  panel with the  $\nu$  and  $\nu$  panels). The ion fraction ( $f_{\text{ion}}$ ) gets much smoother with time. Roughly, the collision rate in the  $\text{HeIV}^+ \rightarrow 2$  jump is large in the shocks, small in cool gas and large in the transition region. The typical three-minute clip (movie) shows  $\nu$  in too fast to permit hydrogen settling: the one shock kink in the temperature and ionization up again before the neutral fraction comes down to the LTE value for the low-post-shock temperature.

In this simulation equal **H<sub>1</sub>** ionizing and deionizing fluxes identified relative balance was assumed for the Lyman formation for transparency. The actual simulation will work the same way as slow recombination, giving larger LTE **H<sub>1</sub>** opacity in cool narrow structures from  $I_{\nu}$  scattering across them. Also for horizontal ones in 3D.

The high green-yellow-orange arcs in the  $\nu$  panel come from cascade recombination where hydrogen ionizes freely. The corresponding arcs in the  $\nu$  and  $\nu$  panels are artifacts from the imposed detailed balancing of  $I_{\nu}$ .

The  $\nu \rightarrow 2$  jump in **H<sub>1</sub>** is 20eV and will similarly affect recombination in cooling gas.

**47**

**H<sub>1</sub> SCATTERING IN A DYNAMIC 3D SIMULATION**

Lecarron et al. (2012)

- H<sub>1</sub>** is a scattering line with  $\tau \approx J$
- $\nu$  behaves qualitatively as in the static 1D models, but with large spread
- across the opacity gap  $J$  is smoothed by 3D radiative transfer
- with 3D smoothing **H<sub>1</sub>** fibrils become visible in stronger field areas
- H<sub>1</sub>** core depth  $\approx$  field density, with  $\nu$  temperature
- H<sub>1</sub>** core depth  $\approx$  aligned with the horizontal field component

**48**

start



index

Results from an important recent paper: [Lemnitz et al. \(2012\)](#) used a snapshot from a 3D0 NE MHD Ohio simulation to synthesize  $H_\alpha$  with 3D radiative transfer (and some reasonable simplifications).

The left-hand graph shows  $H_\alpha$  behavior similar to the ALCT and FCHBF-B models: a flat part across the low-velocity upper photosphere filled with scattered and backscattered radiation, followed by an outward scattering decline. The spread is large but the pattern is the same.

The right-hand images are two synthesized  $H_\alpha$  images, in 3D and 1D (line formation computed along vertical columns as if there were 1D plane parallel stratification, without knowledge of  $L_z$  from other-type columns). I enlarge these images in the next two displays, in reverse order. Blank them and be embarrassed by the subtle appearance of chromospheric fibrils in the center where there is more field in the 3D version. The 3D scattering across the opacity gap obscures the granule-scale field imposed in the photosphere and so enhances the visibility of the fibril scene in the chromosphere. The fibrils aren't yet as clear and abundant as in  $H_\alpha$  observations, but this is their first appearance in an MHD simulation, a triumph.

[Lemnitz et al. \(2012\)](#) added displays which confirm that the  $H_\alpha$  core depth primarily senses density, the core width temperature. In addition, they showed that the fibrils in the 3D image are pretty well aligned with the horizontal component of the magnetic field. Of course, any  $H_\alpha$  image vivifies gives that impression, but it is good to have confirmation of this diagnosis with.

49

CONCLUSION

- chromospheric NLTE
  - chromospheric lines are scatterers
  - even  $H_\alpha$  is a scatterer
  - scattering is beautiful (see Monterey)
- from 1D static SE NLTE to 3D dynamic NE NLTE for  $H_\alpha$ 
  - NE hydrogen ionization balance: large  $H_\alpha$  post-shock opacity
  - $L_y$  scattering: smooth  $H_\alpha$  opacity across small structures
  - special places (deep TR): deuterium radiation  $\nu_{\text{D}}/T_{\text{D}}$  important
- status
  - 1D static modeling serves to study computational line formation
  - 3D line-dependent MHD simulations become more realistic
  - challenge: apply 1D static insights as 3D(1) tricks
- exam
  - Eddington-Barbier as diagnostic for Na I D
  - $H_\alpha$  as diagnostic of field-guided dynamics
  - $H_\alpha$  as diagnostic of field-guided dynamics

52

start



index

Graph: If you passed your finger from the blend at left to the source function at right, equating the blend intensity at left to the source function  $\rightarrow$  Flux function at right in Eddington-Barbier fashion and so concluded that  $\tau = 1$  lies near  $z = 150$  km — then you were a million miles wrong. The blend is a diffuse line, formed by water molecules in our own atmosphere at total height  $h = |h_{\text{air}} - 150| = 150$  km.

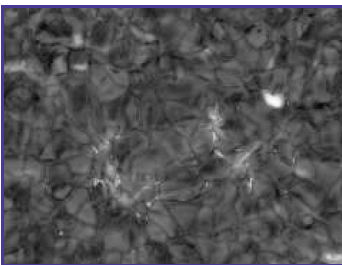
Mean: you have to know the identity and nature of your line and understand its formation before you ask me (or Eddington & Barber) what its formation height is.

Cloud modeling is literally appropriate for this line, not optically-thick stellar-atmosphere modeling. With  $S_{\nu} = J_{\nu}$  and  $\tau = 0$  in the cloud.

Next exam questions: play this [DOT movie](#). What do you see? Where are the gaps? Where is the heart? Why?

55

t thumbs/thumb-\par .jpg



50

start



index

Scattering was the message in this mini-course. The stratified continua are bound-free scatterers. The chromospheric lines are bound-bound scatterers. Even  $H_\alpha$  is primarily scattering and derives its fibril visibility from scattering.

Scattering is beautiful! Watch the ocean, coast, and sky outside the conference room. This beautiful Monterey vista is all scattered sunlight. If you peer a spectroscope at that sea water in the kelp out there, you get to see all Fraunhofer lines. Including  $H_\alpha$ , its core formed in the chromosphere, its wings in the photosphere — while you see it from the sea edge! Even when it is covered without sun in the sky, isn't that wonderful?

Our prospects are excellent. The simulations are getting realistic even for chromospheric fibrils. IRIS will add Mg II h&k as a principal type-B spectral diagnostic to the comprehensive SDO monitoring. I look forward to IRIS spectroscopy of the extreme lines, returning to my original research topic exploring the extended seeing-line observing that space offers over eclipses. For me this very famous offset depicting [Ulrich University anomaly](#) (there were 8 Ulrich alumni here).

Time for the exam in this course. Answer the questions at the bottom of the next display.

If there were a total eclipse right now the *other* would still radiate scattered sunlight containing  $H_\alpha$  but without showing the line. *Continued scattering. Beautiful! Bring a wet cloth to [you]s' constant wetting?*

53

start



index

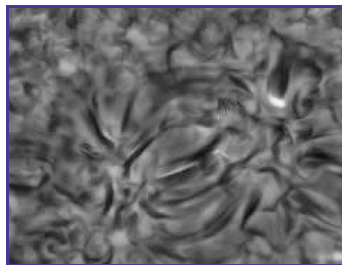
Click on the thumbnail above to download and play the answer movie. If it won't work try the [next version](#). The overlay with TRACE 171 (lower right) was made by [Allied de Wit](#).

The [exam movie](#) (lower-left panel here) shows  $H_\alpha$  Dopplergrams at  $\Delta\lambda = \pm 0.5 \text{ \AA}$ . The maining perpendicular waves are field-guided shocks emanating from sunspot. Even the smallest pores without any discernible penumbra show sunspot penumbra waves as such motions, like the grin of the Cheshire Cat. Their outward expanding field causes these left-to-right spreading Doppler rings.

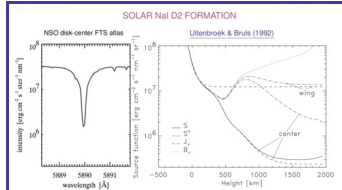
The  $H_\alpha$  core intensity recedes past, [Full-Disk](#) system displays many long fibrils and shorter dynamic fibrils. Darker means larger density. Some have bright undermark, meaning cool. The Doppler movie shows lots of fibril oscillation and flows.

Where is the heart? Obviously in the bright patches in  $H_\alpha$  core intensity that correspond to closely to the bright one-million Kelvin patches in 171. So-called *inos*. Grayscale in the Doppler movie because large thermal broadening diminishes the Doppler visibility. The hot ear-shaped patch left of center is sinking. Its large  $H_\alpha$  brightness must be large  $\partial T/\partial z$  contribution by causal excitation. Presumably because the transition to the corona lies very low. But how and why, and why the very sharp edge-bright boundary? A reconnection front at the near flow? These questions have no answer yet. That's good: something to learn.

56



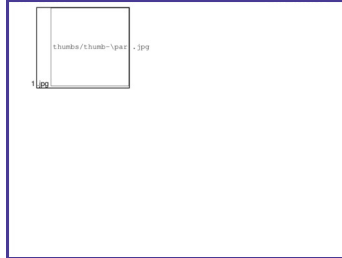
51



Na I D<sub>2</sub> is a fine example of two-level CRD scattering with small  $\epsilon$  in  $\tilde{\mu} = (1 - \epsilon)^2 + \epsilon \tilde{\mu}$ . Eddington-Barbier approximation: pass your finger from line-center  $f(\tilde{\mu}, 1)$  to find that  $S(\tau = 1)$  is at  $h = 600$  km. So: chromospheric velocity but photospheric brightness response.

What is the formation height of the blend at  $\lambda = 5890 \text{ \AA}$ ? What is its  $\tilde{\mu}$ ? Where is the heart?

54



57